

Fly Me to the Moon - For All Mankind

Julius A. Birch

Unaffiliated

(Dated: December 20, 2015)

NASA programme Apollo landed men on the Moon and returned them safely to Earth. In support of their achievements NASA presented, among others, two pieces of evidence which are subject of this report, namely, the photographs of the Apollo 11 landing site; and, the video-recording of the Apollo 17 lift-off.

Starting from post-landing NASA documents, the Apollo 11 landing sequence is proposed in which the Lunar Module cruises at the height of the Lunar Surface Sensing Probes (LSSP, some 1.7 m above the ground) for as much as ten seconds before touchdown, and it is the -Y/Left and +Y/Right landing gears that touched the surface first. This is then compared to pre-landing NASA experimental investigation, according to which the deformation energy $DE \gtrsim KE$, the impact kinetic energy, while the potential energy from settling is the smallest, $PE \ll KE$; and that the one or two gears touching the surface first, absorb most of KE. Contrary to expectations, NASA reported that -Z/Aft landing gear absorbed as much energy as all the other gears combined, and that $DE \simeq \frac{1}{2} KE$. It is shown that this outcome is consistent with the dry Lunar Module being lowered to an uneven surface at near-zero vertical velocity and then released to settle down in Earth-like gravity.

Next, we examine the behavior of the LSSPs in the 360° yaw that the Apollo 11 Lunar Module performed during the Inspection and Separation Stage in the lunar circular orbit. Contrary to NASA's own reference drawings of the fully deployed LSSPs, we find that during the maneuver the LSSPs are always flexed mildly-inwards, as if the Lunar Module were suspended in the presence of gravity, and not weightless in the lunar orbit.

Lastly, detailed analysis of the Apollo 17 lift-off video recording is presented. It is shown that the vessel trajectory implies an additional propulsion in form of an explosion, while the video frames flicker at 5 Hz and 10 Hz rate and carry an artefact strongly resembling an edge of film stock. An analysis of illumination of the ascending Lunar Module is also presented, which suggests that the vessel is approaching near-by light source rather than being lit by the Sun (at infinity). A discussion of the entire scene follows, and an explanation for the explosion is proposed.

Overall, it is concluded that the photographs and the video recording depict scenes that were staged here on Earth, rather than on the way to the Moon.

Contents

1. Who's that flyin' up there?	3
1.1. Liftoff in Theory	3
1.2. Liftoff Curve	6
1.3. Results and Discussion	7
1.4. Tables and Figures	10
2. And shake a leg, Shake a leg, Shake a leg, Shake it again	16
2.1. The Apollo 11 Landing	16
2.1.1. TN D-6850	16
2.1.2. Photographs	18
2.1.3. Voice Transcripts	20
2.1.4. Blanchard's Findings	21
2.2. Discussion and Conclusions	22
2.3. Discussion and Conclusions	24
2.4. Tables and Figures	27
3. Also sprach Zarathustra	31
3.1. Film Stock	31
3.2. Flicker	31
3.3. Space Rocket or Space Elevator?	32
3.4. Heading for the Light	33
3.5. Baby, you are firework!	35
3.6. Conclusions	36
3.7. Tables and Figures	37
4. Standing In Motion	44
4.1. LSSP Equilibrium Position at Rest with Hinge as Pivot	44
4.2. Results and Discussion	46
5. I know you can't fake it anymore	49
Acknowledgments	49
References	50

1. WHO'S THAT FLYIN' UP THERE?

Liftoff of the Apollo 17 Lunar Module on December 9, 1972, from Taurus-Littrow Valley on the Moon was recorded by a video camera on the Lunar Roving Vehicle (LRV). The LRV was parked some 120m eastward on the side of a hill, as shown in Fig.1 from Ref. [1]. The LRV was positioned at higher ground than the Lunar Module, with the Sun approximately behind the camera. We remark that in the NASA reference images of the landing site [2] the Sun is in the west. Interestingly, the camera, which could zoom-out and tilt, was remotely controlled by the Earth ground control [3].

Since the 1970's, speculations have been circulating in the public as to whether the video recording shows liftoff of the Apollo 17 Lunar Module from the Moon, or a staged event occurring elsewhere. something else somewhere else. Some of these speculations can be put to rest through analysis of the video recording of the liftoff.

The purpose of this section is to extract the first 2 seconds of the liftoff dynamics of the Apollo 17 Lunar Module Ascent Stage (LMAS) from the video recording, and to compare it to the values published by NASA in different media. Starting from the equation of motion of a rocket lifting off a planetary surface, we introduce assumptions that allow us to write its short-time solution as a special third- and forth-degree polynomial in time which we call the Jerk (J) and the Snap/Jerk (S/J) model, respectively. The short-time solution then influences the parameters of the constant acceleration motion, which is the long-time solution. We then analyze 21 frames extracted from the video recording at the rate of 10 frames-per-second (fps), to find the height the LMAS gains as a function of time, the so-called, "liftoff" curve. Finally, by fitting the models to the liftoff curve, we find the propulsion parameters and discuss the dynamics of liftoff the video recording depicts.

1.1. Liftoff in Theory

The one-dimensional rocket equation is a standard fare in any text-book on analytical mechanics [4]. Here, we are interested in a rocket lifting off a planet that provides constant gravity g . Let the rocket mass be $m = m(t)$, and let the propellant be expelled from the rocket engine combustion chamber at mass rate $\dot{m}_p(t)$ with the velocity w relative to the rocket. We assume that the planet has no atmosphere, so the motion is described in terms of the rocket vertical velocity $v = v(t)$

as, [5]

$$\dot{v} = \frac{\dot{m}_p w}{m(t)} + \frac{p_e A_e}{m(t)} - g. \quad (1.1)$$

We remark while the rocket is sitting on the ground the right-hand-side of Eq. (1.1) cannot be smaller than zero, meaning that the rocket remains stationary on the surface. Here, p_e is the pressure of the propellant at the exit of the nozzle, while A_e is the surface of the nozzle at the exit. We simplify Eq. (1.1) as,

$$\dot{v} = \frac{F_{th}(t)}{m(t)} - g, \quad (1.2)$$

where $F_{th} = F_{th}(t)$ is the engine thrust in vacuum, which we allow to vary in time.

For the purpose of our analysis, we split the liftoff dynamics to the initial short-time period, and the subsequent long-time period. We refer to the initial short-time period as the “warm-up”. Let us assume that the vessel is initially at rest, and that its rocket engine starts propulsion at time $t = 0$. This is not necessarily the time at which the liftoff starts as it may take time for the rocket engine to produce enough thrust to counter-act gravity. We introduce the warm-up time $t_1 \geq 0$, at which the rocket engine reaches its full (maximal) thrust. The time instant t_1 thus separates the short-time from the long-time period.

First we approximate the warm-up through $F_{th}(t)$ linearly increasing for the duration of warm-up time t_1 and as constant P thereafter,

$$F_{th}(t) = \begin{cases} 0, & \text{for } t \leq 0 \\ \frac{P}{t_1} \cdot t, & \text{for } 0 \leq t \leq t_1, \\ P & \text{for } t_1 \leq t. \end{cases} \quad (1.3)$$

The liftoff starts when the rocket begins to move at time t_0 , such that $F_{th}(t) \geq m(t)g$, for $t \geq t_0$. From our linear model of thrust we find $t_0 \approx m g t_1 / P$. For comparison, [6] the Ascent Propulsion System (APS) featured in the Lunar Modules of the Apollo missions had only “on” and “off” states, where the transition between the two states occurred in near step-like fashion with the delay time of 0.3 s. In terms of our linear model (1.3) this is written as $t_0 \approx t_1 \approx 0$, with P/t_1 some large number, where the start command to the engine was issued at $t' \approx -0.3$ s.

From the properties of the APS [7, 8], some of which we summarize in Tbl. I, we can neglect the change in the total mass of the LMAS for the 2 seconds of liftoff we are interested in, and so

approximate the LMAS mass with its initial mass $m(t) \approx m_0^{AS}$. This allows us to find the vertical acceleration of the LMAS \dot{v}_A as,

$$\dot{v}_a(t) = \begin{cases} 0, & \text{for } t \leq t_0 \\ j_A \cdot (t - t_0), & \text{for } t_0 \leq t \leq t_1, \\ j_A \cdot (t_1 - t_0), & \text{for } t_1 \leq t. \end{cases} \quad (1.4)$$

where we have introduced *jerk*, $j = d^3x/dt^3$. We refer to Eq. (1.4) as the J-Model of warm-up. After the warm-up time, $t \geq t_1$, the ascent continues with approximately constant acceleration,

$$a_{max} = j_A \cdot t_1 = \left(\frac{F_{th}}{m_0^{AS} g} - 1 \right) \cdot g \approx 1.95 \text{ m} \cdot \text{s}^{-2}. \quad (1.5)$$

Because of $t_0 \approx t_1 \approx 0$, in Apollo 17 liftoff a_{max} is achieved immediately. As at time $t = 0$ the LMAS is at rest, its vertical position is thus described by

$$X(t) = \frac{a_{max}}{2} t^2. \quad (1.6)$$

In their numerical simulation of Apollo 17 lunar orbit insertion Braeunig [9] reports $X(2 \text{ s}) = 3.0 \text{ m}$, whereas Eq. (1.6) reads $X(2 \text{ s}) \approx 3.9 \text{ m}$. This implies that in Braeunig's simulation the Ascent Propulsion System transitions from zero to full thrust with a delay of 0.25 s, in full accord with [6].

Next we anticipate that the J-Model of the rocket engine thrust might not be sufficient, because it constrains the warm-up transients to $j \geq 0$. One way to better capture the transients is to introduce an additional parameter *snap*, $s = \frac{dj}{dt}(t) = \frac{d^2\ddot{x}}{dt^2}(t)$, so that the acceleration during warm-up is:

$$\dot{v}_a(t) = \begin{cases} 0, & \text{for } t \leq t_0 \\ \frac{s}{2}(t - t_0)^2 + j \cdot (t - t_0), & \text{for } t_0 \leq t \leq t_1, \\ \frac{s}{2}(t_1 - t_0)^2 + j \cdot (t_1 - t_0), & \text{for } t_1 \leq t, \end{cases} \quad (1.7)$$

which we refer to as the S/J-Model of warm-up.

Finally, the long term behavior that ensues following the warm-up is best described by the constant acceleration motion,

$$x(t) = \frac{1}{2} \ddot{x}(t_1) (t - t_1)^2 + \dot{x}(t_1) \cdot (t - t_1) + x(t_1), \text{ for } t > t_1, \quad (1.8)$$

where its parameters, namely $\ddot{x}(t_1)$, $\dot{x}(t_1)$ and $x(t_1)$, are fully determined by the warm-up.

When fitting the liftoff curve to the models we see that the J-Model (1.4) has three parameters (j, t_0, t_1) , the S/J-Model (1.7) has four (s, j, t_0, t_1) , as does the constant acceleration model $(t_1, \ddot{x}_1(t_1), \dot{x}_1(t_1)$ and $x_1(t_1))$. In other words, even though the S/J model appears to be more complicated than the constant acceleration motion, they both have the same number of parameters.

1.2. Liftoff Curve

Processing of Images: The web site YouTube provides the video recording of Apollo 17 liftoff [10] in Adobe-Flash format. We use another web service [11] to download it for us, and to convert it to AVI format. The converted file is then downloaded to our workstation under the name `Apollo_17_Lunar_Liftoff_high.avi`. We analyze the file using the software package FFmpeg [12], and find it comprised of color images 480x360 (width-by-height) pixels recorded at rate $r = 25$ fps. We then convert the video recording to a set of images at the rate $r = 10$ fps [46]. As a result of conversion, we get the images numbered 1,2,3..., where the increments of 1 indicate the time stamp of an image to be $\Delta t = 1/r$ greater than the previous one, with image 00001 being the first. Accordingly, one can determine the absolute time stamp of the image in the video recording as $(n - 1)/r$, where n is the index image. We find that at the rate $r = 10$ fps, the first two seconds of liftoff are depicted in 21 images numbered $[363 : 383]_{10}$ [47], where the subscript next to the image number or range indicates the extraction rate. For the reader's convenience, in Fig. 2 we provide the reference image 363_{10} , while in Fig. 3 we combine the images $[364 : 383]_{10}$.

We choose as $t = 0$ the image 363_{10} as in the subsequent images the motion of the LMAS is obvious and the Moon surface disappears in the dust cloud. Simultaneously, the images 364_{10} onward begin to show the effects of a continuous zoom-out. [13]

We limit our analysis to the first 2 seconds, as after that point the camera begins to tilt.

Extraction of liftoff curve: In each of the images $[363 : 383]_{10}$ we locate 5 points:

H_1 horizon point No. 1, on the left from LM where the ridge lines of the left hill (presumably, Horatio) and of the right hill (presumably, Camelot) meet;

H_2 horizon point No. 2, on the right from LM at the top of the right hill (Camelot);

L_1 leg point No. 1, bright section at the top of the left leg of the LMDS when facing it on the picture;

M_1 LMAS point No. 1, top left corner of the bright surface of the AS;

M_3 LMAS point No. 3, bottom left corner of the bright surface of the AS.

In Fig. 2 we show these five points on the reference image 363₁₀. In Tbl. II we give the Y-pixel coordinates of each of these five points for images [363 : 383]₁₀, which we have extracted using the software package GIMP [14].

We first establish how do vertical distances between fixed objects L_1 , H_1 and H_2 vary in time. For that purpose we construct two data sets, $DY_{1,2} = Y(L_1) - Y(H_{1,2})$, which we fit to

$$DY_{1,2}(t) = k_{1,2} \cdot (t_{inf} - t). \quad (1.9)$$

We remark that since two distances satisfy Eq. (1.9), throughout the zoom-out the ratio of the distances is fixed,

$$\frac{DY_1}{DY_2}(t) = \frac{k_1}{k_2}, \text{ not a function of time,} \quad (1.10)$$

so either can be used for measuring all the other distances. From the data in Tbl. II, which is plotted in Fig. 4, we find $k_1 = 7.8 \pm 0.2 \text{ s}^{-1}$, $k_2 = 22.3 \pm 0.5 \text{ s}^{-1}$, and $t_{inf} = 6.5 \pm 0.1 \text{ s}$. The metric function thus reads $\mu_{363}(t) = 1p_{363} \times (1 - t/t_{inf})^{-1}$. From [15], p.1-4, we find that the height of the Lunar Module Ascent Stage at the top of the Descent Stage is 2.83 m. From the image 363₁₀ we find this distance to be 70 pixels, so $1p_{363} = 4.0 \text{ cm}$. This allows us to find the liftoff curve, which we provide in Tbl. III and plot as black circles in Fig. 5.

1.3. Results and Discussion

We find the best-fit parameter estimates using the least-squares method. For the S/J Model (1.7) we find:

$$\begin{aligned} \hat{t}_0 &= 0 \text{ s,} \\ \hat{t}_1 &= 0.29 \pm 0.07 \text{ s,} \\ \hat{j} &= 104 \pm 35 \text{ m} \cdot \text{s}^{-3}, \\ \hat{s} &= -673 \pm 385 \text{ m} \cdot \text{s}^{-4}. \end{aligned} \quad (1.11)$$

As can be seen from Fig. 5, the S/J Model (position in red, acceleration in orange) fits the liftoff curve quite nicely over the entire data range.

We extract the parameters of the constant acceleration motion, Eq. (1.8), where we set $t_1 \equiv 0.3 \text{ s}$,

as

$$\begin{aligned}
 \hat{a}_1 &= 2.00 \pm 0.50 \text{ m} \cdot \text{s}^{-2}, \\
 \hat{v}_1 &= 1.03 \pm 0.60 \text{ m/s}, \\
 \hat{x}_1 &= -0.15 \pm 0.33 \text{ m},
 \end{aligned}
 \tag{1.12}$$

where $x(t) = \frac{1}{2}\hat{a}_1 t^2 + \hat{v}_1 t + \hat{x}_1$, that is, without offset by t_1 . The acceleration \hat{a}_1 is in excellent agreement with the expected $a_{max} = 1.95 \text{ m} \cdot \text{s}^{-2}$. For reference we plot Eq. (1.6) in Fig. 5, with position in pink and acceleration in magenta.

As discussed earlier, the warm-up time of the rocket engine (first warm-up time) ended by the time $t = 0$ when the AS started to move. However, the S/J Model suggests that during the second warm-up time, from 0 to $t_1 \simeq 0.3 \text{ s}$, the Ascent Stage was under influence of a very strong force, which subsequently vanished. This force was responsible for the long-term velocity $\hat{v}_1 \simeq 1 \text{ m} \cdot \text{s}^{-1}$. Because the strong force vanishes after t_1 , the J-Model cannot appropriately describe the motion under its influence.

We argue that the long-term velocity \hat{v}_1 is not an artifact of improperly compensated zoom-out, but the true feature of the liftoff. To see that, one must recall that zoom-out shrinks the distances in a non-linear fashion, so that the velocity and acceleration are modified, and not just the velocity,

$$x(t) = 1p_{363} \cdot \frac{DY(t)}{1 - \frac{t}{t_{inf}}} \simeq 1p_{363} \cdot DY(t) \cdot \left(1 + \frac{t}{t_{inf}} - \frac{t^2}{2t_{inf}^2} \right).
 \tag{1.13}$$

As we find acceleration from the converted liftoff curve to be exactly what we expected, we conclude that the non-zero velocity is not an artifact of conversion, but a feature of the liftoff.

The short burst of force is consistent with an explosion, which produces peak thrust of $F_a \simeq 27 \text{ kN}$ some $\sim 0.15 \text{ s}$ after the LMAS starts to ascend. For comparison, the rocket engine produces thrust $F_{th} = 2.2 \cdot m_0^{AS} g \simeq 16 \text{ kN}$. Here, we remark that the crew used explosive devices in preparation for liftoff to separate the electrical and mechanical connections between the stages, and to vent the DS fuel tanks so they would not ignite during liftoff. These devices, however, would be activated in preparation for ascent- not after the Ascent Propulsion System was started. Coincidentally, the frames 365₁₀ (+0.2 s) onward, in Fig. 3, suggest a visible explosion taking place between the Ascent and the Descent Stage as they separate: The amount of flying debris and its brightness is maximal in the frame 366₁₀ (+0.3 s) and subsides thereafter. On the ApolloHoax.net discussion thread [16] it was proposed that the visible explosion provided additional propulsion through the Jules Verne's "bullet in the barrel" launching method. This argument is flawed, as the

rocket engine immediately blows dust from the surface, making build-up of exhaust gas pressure unlikely anywhere in the Descent Stage (DS). In addition, the empty volume in which the nozzle sits in the DS that could potentially serve this purpose is not in any way structurally reinforced to sustain such pressures. It is also rectangular in shape which directs gas flow toward the edges, making them fall apart (and so let the gas inside the DS).

The explosion appears to be an unplanned event, thus its direction and magnitude must be random. Asymmetry of the explosion would destabilize the vessel, appearing as forced change in roll or pitch angle or rate. It is established that the rocket is marginally stable with respect to small changes in roll or pitch angle φ ; unless counteracted by the Abort Guidance Section (AGS) [17] the roll or pitch motion introduced by the explosion would continue unhindered. The lateral acceleration of the vessel would then become:

$$\ddot{y} = \sin \varphi \cdot \frac{F_{th}}{m}. \quad (1.14)$$

For example, 1° un-compensated pitch for a duration of 2 seconds causes the vessel to move laterally by $y \approx 12$ cm, and to continue drifting at $\dot{y} \approx 12$ cm/s. This lateral motion would be easily visible on the video recording with its ~ 4 cm/pixel resolution. We remark that the AGS cannot counteract such minute lateral motion because it is below its detection thresholds. It is also unnecessary considering its goal of meeting with the Control and Service Module (CSM) in lunar orbit.

1.4. Tables and Figures

Name	Quantity	Value
Lunar gravity	g	1.622 m·s ⁻²
Ascent Stage height	l_{AS}	3.76 m
Descent Stage height	l_{DS}	3.23 m ^a
Ascent Stage mass (dry)	m_d^{AS}	2132 kg
Ascent Stage propellant mass	m_p^{AS}	2359 kg
Ascent Stage total mass	m_0^{AS}	4491 kg
Descent Stage mass (dry)	m_d^{DS}	2767 kg
Lunar Module Earth Launch	m^{LM}	16375 kg
Landing Mass	$m_{LM} \approx m_0^{AS} + m_d^{DS}$	7258 kg
APS Thrust	F_{th}	16,000 N
Propellant expelled velocity	w	3050 m/s
APS Thrust-to-Weight at Liftoff	$\alpha = F_{th}/(m_0^{AS} \cdot g)$	2.20

^aThis assumes un-deployed primary struts. See discussion in the text.

TABLE I: Relevant Lunar Module Data for Analysis of Liftoff. [7, 8]

Image No.	$Y(H_1)$	$Y(H_2)$	$Y(L_1)$	$Y(M_1)$	$Y(M_2)$
363	296	246	150	236	271
364	295	245	150	234	268
365	294	244	151	233	265
366	291	243	152	229	263
367	290	243	153	224	254
368	289	241	153	220	249
369	286	239	154	212	243
370	284	239	155	208	236
371	282	238	155	200	230
372	280	237	156	194	224
373	278	235	156	187	217
374	277	234	156	183	210
375	275	234	158	175	203
376	274	233	158	168	197
377	272	231	158	162	189
378	272	231	159	155	182
379	269	230	160	148	174
380	267	230	160	142	168
381	267	228	160	133	159
382	264	227	161	127	153
383	264	227	161	120	145

TABLE II: Pixel Y-coordinates of the reference points on the Lunar Module and the Moon landscape in the images $[363 : 383]_{10}$. The reference points are shown in Fig. 2, while the images are combined in Fig. 3.

Time (s)	Ascent (m)
0.0	0.00
0.1	0.08
0.2	0.12
0.3	0.20
0.4	0.42
0.5	0.59
0.6	0.87
0.7	1.02
0.8	1.35
0.9	1.61
1.0	1.92
1.1	2.14
1.2	2.53
1.3	2.92
1.4	3.23
1.5	3.71
1.6	4.05
1.7	4.40
1.8	5.05
1.9	5.38
2.0	5.96

TABLE III: First two seconds of liftoff of the Apollo 17 Lunar Module Ascent Stage.

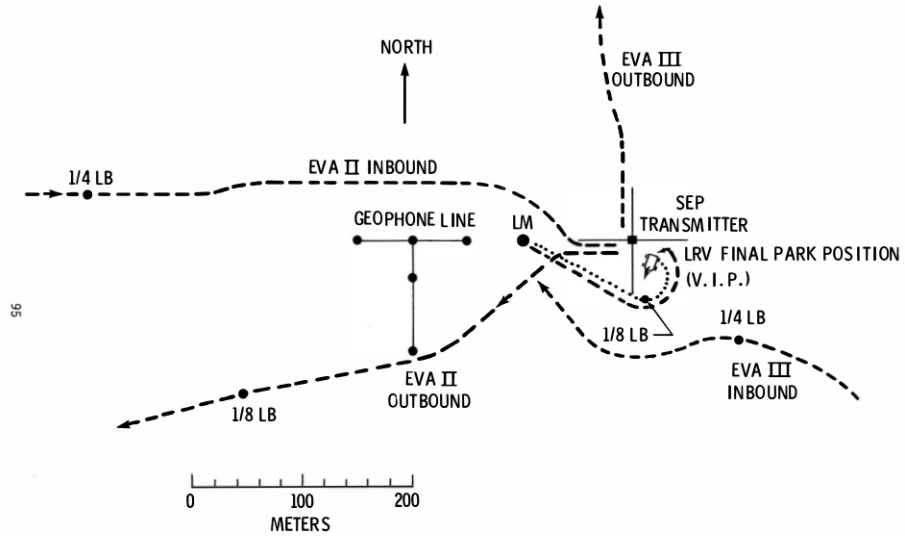


FIG. 1: The map of the Apollo 17 landing site on the Moon [1] shows the location of the Lunar Roving Vehicle (LVR), which carried the remote-controlled camera that recorded the liftoff.

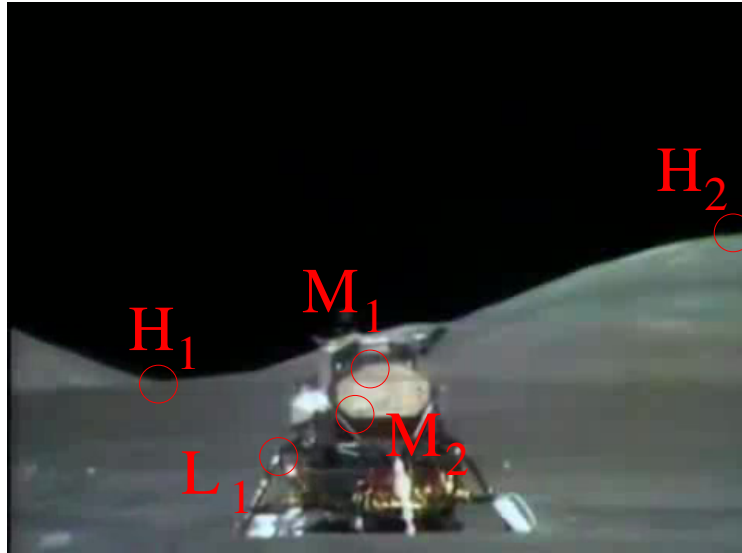


FIG. 2: The reference points on the Lunar Module and the Moon landscape in the image 363_{10} that are used for extraction of liftoff curve.

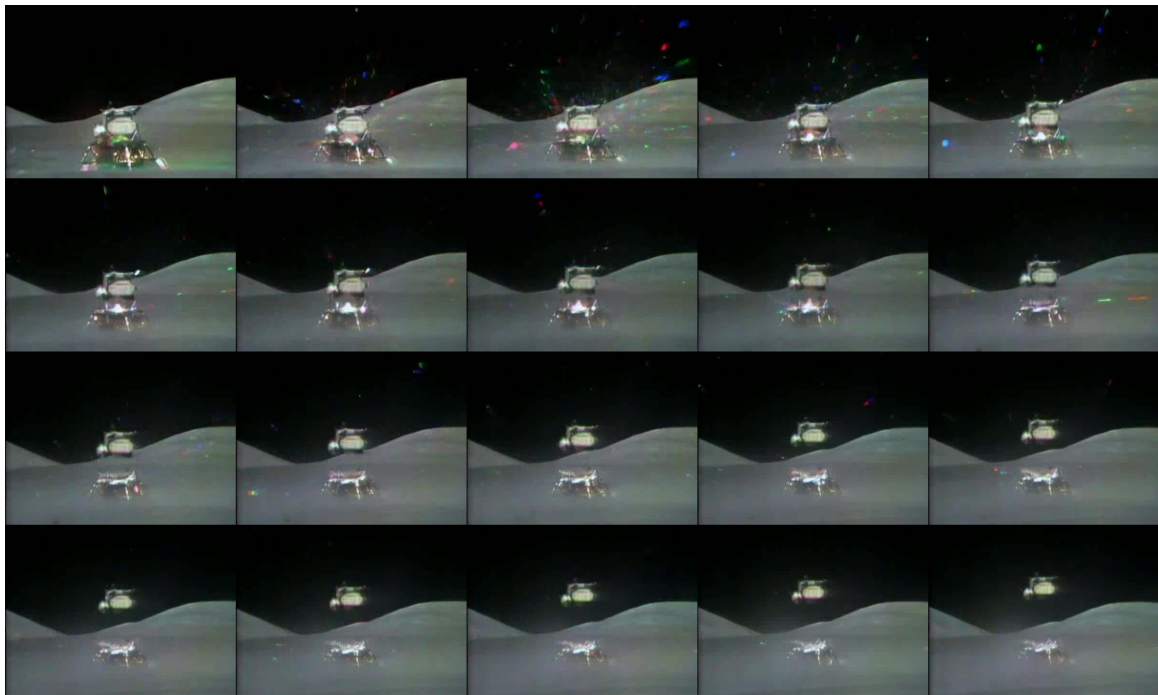


FIG. 3: Composition of the images $[364 : 383]_{10}$, which are used for extraction of Y-pixel positions of the reference points. The image numbers go left-to-right, top-to-bottom, and are spaced at 0.1 second interval. The extracted positions are given in Tbl. II.

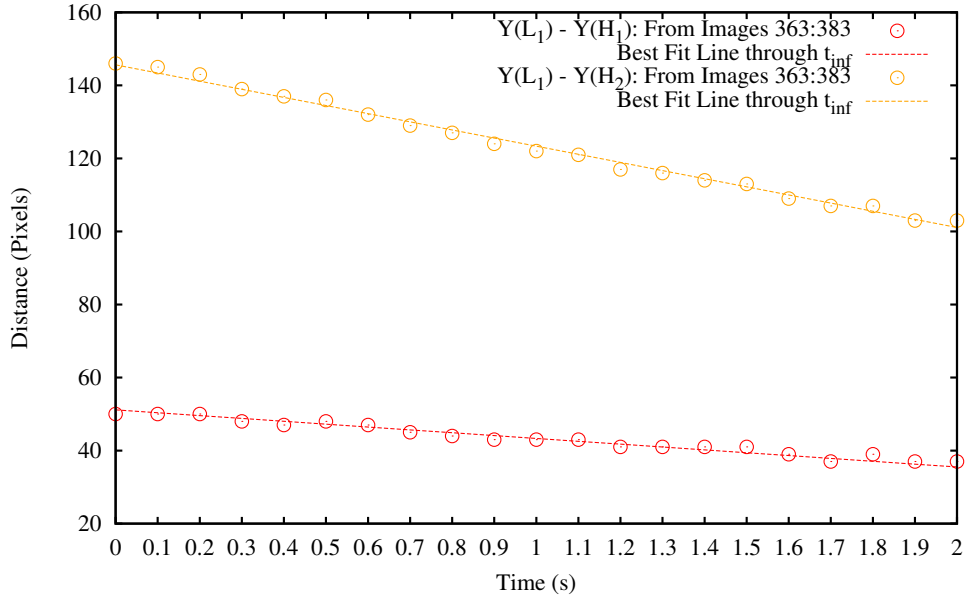


FIG. 4: Vertical distance in pixels between the reference points in images $[363 : 383]_{10}$ with the best-fit linear models used for removal of camera zoom-out.

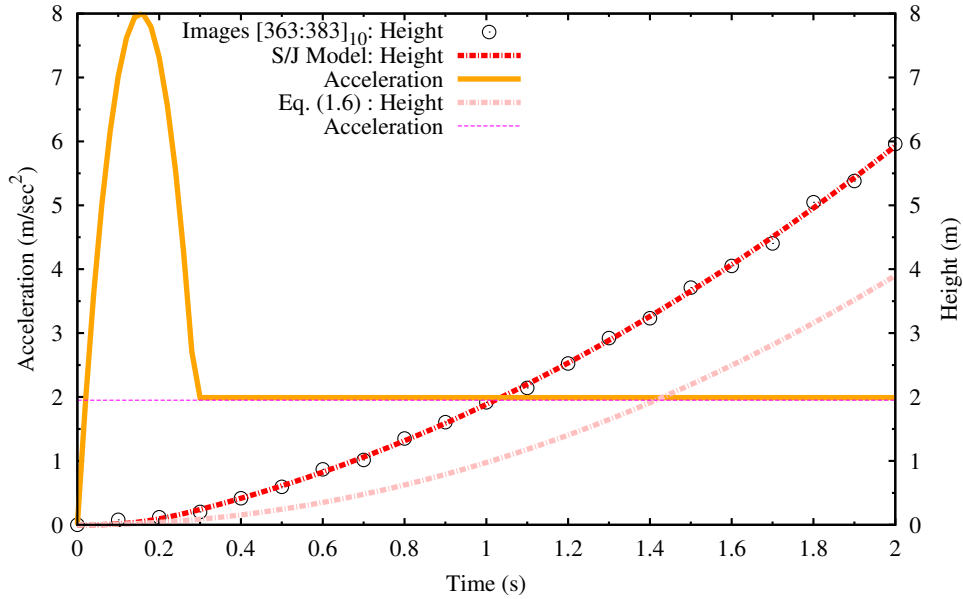


FIG. 5: Apollo 17 Lunar Module Ascent Stage liftoff curve from Tbl. III (black circles), does not match the constant acceleration motion starting from rest (position in pink, acceleration in magenta) given by Eq. (1.6) except in the acceleration of the ascent. The S/J model (position in red, acceleration in orange) besides fitting the liftoff curve well, also suggests an explosion taking place in the first 0.3 seconds of liftoff, which gives the Ascent Stage extra velocity of $v_0 \simeq 1$ m/s.

2. AND SHAKE A LEG, SHAKE A LEG, SHAKE A LEG, SHAKE IT AGAIN

We focus next on the deployment of landing gears in the Apollo 11 and 17 missions. The sketch of one landing gear is shown in Fig. 6. The primary and secondary struts (PS,SS) are the crucial elements of the landing gear. Their purpose is to attenuate the impact of landing on the lunar surface. The struts are piston-cylinder type; they absorb compression (PS, SS) or tension (SS) load of the lunar landing and support the Lunar Module (LM) on the lunar surface. The loads are attenuated by a crushable aluminum-honeycomb cartridge in each strut. [7] While the primary struts may shorten under compression loads, the secondary struts may shorten or elongate as a result of deployment.

There are two NASA technical notes concerned with the landing gear that are of interest here. The first is the Blanchard's investigation of the lunar module prototype landing gear that was performed at the Langley Research Center in simulated Moon gravity, Technical Note TN D-5029 [18] from March, 1969.

2.1. The Apollo 11 Landing

2.1.1. TN D-6850

In Technical Note TN D-6850 [19], dated June 1972, Rogers presented post-flight analysis of the Apollo 11 Landing Gear Subsystem performance in landing on the Moon. The analysis is based on the photographs of the landing gear that were returned from the mission and collected instrumental data.

Firstly, it is reported that the Apollo 11 Lunar Module underwent powered descent. In touch-down the (vertical) impact velocity was $v_x = -0.55 \text{ m}\cdot\text{s}^{-1}$, while the horizontal velocity was $v_y = -0.67 \text{ m}\cdot\text{s}^{-1}$ in -Y direction. From the landing mass of the Lunar Module $m_{LM} = 7258 \text{ kg}$, the total kinetic energy is $\text{KE} = 2.7 \text{ kJ}$, where the vertical part is $\text{KE}_x = 1.1 \text{ kJ}$ and the horizontal $\text{KE}_y = 1.6 \text{ kJ}$.

Secondly, from the photographs of landing gears it is found that the primary struts underwent no compression, that is, did not absorb any impact energy (one may wonder why this is repeated four times in single section of the report). Similarly, it was found that the secondary struts underwent only tension load, as a result of which they elongated. The reported tension strokes of the secondary struts are reported in the second column of the following table,

Secondary Strut Id.	Stroke ^a Δs (mm)	Deformation Energy ^b (kJ)	Deformation Energy ^c (kJ)
+Z[Front]/R	0		
+Z[Front]/L	102	0.2	
-Z[Aft]/R	64		
-Z[Aft]/L	114	0.7	0.4
+Y[Right]/R	71		
+Y[Right]/L	13	0.2	
-Y[Left]/R	81		
-Y[Left]/L	0	0.2	

^aTension.

^bUsing Rogers' average values from Eq. (2.1).

^cSame, but assuming single tension zone over the entire elongation.

In the third column, the deformation energy absorbed per landing gear is estimated, and the total found to be $\Phi_2 \simeq 1.3$ kJ. These estimates are based on the average secondary strut tension reported in TN D-6850,

$$F_2(\Delta s) = \begin{cases} 2.2 \text{ kN}, & \text{for } \Delta s \leq 0.10 \text{ m} \\ 22.2 \text{ kN}, & \text{for } 0.1 \text{ m} \leq \Delta s. \end{cases} \quad (2.1)$$

In the fourth column, the deformation energy of the -Z[Aft]/Left strut is calculated assuming $F_2(\Delta s) \simeq 2.2$ kN, for all Δs . In this case, the total deformation energy absorbed in the secondary struts is $\Phi'_2 \simeq 1$ kJ.

Lastly, for reader's convenience the scaled strokes of secondary struts with their approximate directions are given in Fig. 8, together with the direction of vertical velocity in touchdown. What is important to notice is that based on the horizontal motion in -Y direction the landing was of, so called, 1-2-1 type. Based on Rogers values 3 s before touchdown of pitch $\varphi \approx 4^\circ$ and roll $\theta \approx 0^\circ$, (Fig.16, p.17), the footpads $\pm Y$ were displaced by $\Delta X_{\pm Y} \approx \mp \frac{1}{2} l \cdot \sin(\theta) = \mp 0.32$ m from the center (minus sign means the footpad was below, while plus sign above local instrumental horizontal). Here, $l = 9.45$ m (=31 ft) is the distance between the $\pm Y$ or $\pm Z$ footpads. Thus +Y footpad was coming down first, followed by $\pm Z$, while the -Y footpad was the last. At touchdown the LM conformed with the surface, where pitch angle dropped to $\varphi \approx 0.8^\circ$, indicating almost flat surface along $\pm Y$ direction (0.13 m vertical difference over l), but the roll angle increased to $\theta \approx 2.6^\circ$ suggesting an incline in $\pm Z$ direction where the +Z touchdown point is some 0.42 m above the -Z one. Few seconds after touchdown, the LM settled at pitch $\varphi \approx 5^\circ$ and roll $\theta \approx 0^\circ$.

In the absence signs of compression in all gears, from the attitudes of the LM during the landing, one can conclude that

- the +Y gear should elongate substantially over the -Y gear, to the effect of creating a 5° pitch on the flat surface in $\pm Y$ direction; and,
- the +Z gear should elongate somewhat, so that the negative roll of the Lunar Module counteracts 2.6° inclination of the surface in $\pm Z$ direction.

In terms of deformation energy absorbed by individual landing gears under a constraint of no-compression, the +Y should absorb the most energy, +Z somewhat less, while -Y and -Z very little. In addition, +Y gear would absorb most of the horizontal kinetic energy at impact being the first to touchdown.

Conversely, the energy disipation from Rogers measurements of the strut strokes suggests that it is the -Z gear that absorbs the most, while all the others absorb approximately the same amount of energy.

2.1.2. Photographs

Consider four photographs in Fig. 7 that were taken following the landing. The photograph AS11-40-5858 [20, 21] (top left) and AS11-40-5864 [20, 22] (top right) show the +Y[Right] footpad, and the rocket engine nozzle and the lunar surface below it. The photograph AS11-40-5865 [20, 23] (bottom left) shows the -Y[Left] footpad, while the photograph AS11-40-5921 [20, 24] (bottom right) shows the rocket engine nozzle and the lunar surface below it. Their combination suggests that the drag marks of the +Y[Right] and -Y[Left] LSSP's may have been longer than the horizontal distance the LM can cover in 3 s ($\simeq 2$ m) while moving with the touchdown horizontal velocity of $v_y = -0.67 \text{ m}\cdot\text{s}^{-1}$.

Firstly, AS11-40-5858 shows the +Y[Right] LSSP traveling some 2.5 m. Assuming touchdown horizontal velocity of $v_y = -0.67 \text{ m}\cdot\text{s}^{-1}$ and a horizontal coast with $\theta = 5^\circ$ pitch, which produces acceleration $\ddot{y} \approx -g \sin \theta = -0.14 \text{ m}\cdot\text{s}^{-2}$, prior to landing, it takes ~ 2.9 s to cover 2.5 m. Interestingly, this suggests that the horizontal velocity at the the beginning of the drag mark was $-1.1 \text{ m}\cdot\text{s}^{-1}$ ($\approx 3.6 \text{ ft/s}$), which is awfully close in magnitude to the maximum allowable horizontal landing speed of $1.2 \text{ m}\cdot\text{s}^{-1}$ ($=4 \text{ ft/s}$). Conversely, if we neglect the pitch of the LM, covering the same distance requires ~ 3.7 s.

Secondly, the images AS11-40-5865 and AS11-40-5921 suggest that the -Y[Left] LSSP drag mark starts from the outside the nozzle on the side of +Y[Right] footpad and is at least 5.5 m long ($=31'58''/2$), suggesting the travel time of some ~ 5.3 s considering the pitch, or ~ 8 s without. As

shown in AS11-40-5921 and illustrated in Fig. 8, only the section of the drag mark directly under the nozzle appears to have been erased. It is puzzling that the drag mark appears not to be blown away but covered with sand considering there was an rocket engine operating above it.

Furthermore, in AS11-40-5858 [20, 21] in front of the +Y[Right] footpad there is a trace that is in the direction of the -Y[Left] footpad, and which appearance is consistent with that of a drag mark. It is interesting that for these three marks to belong to -Y[Left] LSSP the LM must have made slight clock-wise yaw after making the first mark (by the +Y[Right] footpad). In that case the total distance covered by the -Y[Left] LSSP is some 9.4 m, which requires travel time of ~ 7.8 s with the pitch, or ~ 14 s without. Again, it is puzzling that this drag mark was not erased by the operating rocket engine passing above it at the height of the LSSPs.

Lastly, the Rogers deformation energies per landing gear suggest -Z absorbing the most. Fig. 9 shows the photographs AS11-40-5914 [20, 25] (Left panel) and AS11-40-5920 [20, 26] (Right panel) of the -Z[Aft] landing gear. The photographs show that the final resting position of the -Z[Aft] LSSP was radially outwards from the LM center (that is, in the -Z direction), rather than opposite the horizontal direction of motion at landing (which would be in +Y direction). Then, on AS11-40-5920 one can observe a mound under the footpad also on the side of the LM center. The two together would suggest that at touchdown the LM was travelling in the +Z direction, which contradicts all the other data (and the -Y directed horizontal motion at touchdown).

As a side comment, from the photograph AS11-40-5921 the distance between the nozzle center and its projection on the lunar soil is found to be $h' = 0.42$ m by comparison to the radius of the nozzle of $R_n = 0.74$ m (=29"). This value substantially improves on Rogers estimate $h'_{Rog} = 0.34$ m (=13.5", [19], Fig.17 on p.20). From the specifications of the Lunar Module, the height from the lower edge of the nozzle to the bottom of the footpads is $h = 0.47$ m (=1'6.48"). If the LM landed on perfectly flat surface without lateral motion, this would indicate that during settling its center-of-mass dropped in height by $\Delta h = h - h' = 5$ cm. This provides an estimate for the gravitational energy from settling ΔPE ,

$$\Delta PE \approx m_{LM} g_{local} \Delta h, \quad (2.2)$$

that contributed to the impact kinetic energy in overall energy balance equation of landing in local gravity g_{local} . For the Moon landing one finds, $\Delta PE \simeq 0.6$ kJ. For comparison, were Rogers correct this would be $\Delta PE_{Rog} \simeq 1.5$ kJ.

2.1.3. Voice Transcripts

From the voice transcripts of the communication during the landing [27] it transpires that between the Lunar Surface Sensing Probes (LSSP) touching the lunar surface (at GET 102:45:40 “Contact Light” was apparently called) to the announcement of “Shutdown,” 3 seconds passed. As the LSSPs length is ~ 1.7 m, the average impact velocity in this scenario, $1.7/3 \simeq 0.57$ m·s⁻¹, is consistent with Rogers’ v_x .

In the following table the data announced by the crew over the last 61 m (200 ft) of descent is listed. In the first column is the Ground Elapsed Time (GET), while in the second is the time passed since the crew reported reaching the 62 m (=200 ft) height. If the third (fourth) column is not empty, it contains the height in feet (meters) reported by the crew. With the entries in fifth column that contain sink rates, the descent data reported by the crew concludes. In the sixth column are the average sink rates calculated between the consecutive times and heights reported by the crew.

GET (hrs)	Rel. Time (s)	Height (ft)	Height (m)	Sink Rate (m/s)	Avg. Sink Rate (m/s)	Guessed Sink Rate (m/s)
102:44:24	0	200	61.0	-1.4		
102:44:26	2			-1.7		
102:44:31	7	160	48.8	-1.9	-1.7	
102:44:33	9			-1.7		
102:44:40	16	120	36.6		-1.4	
102:44:45	21	100	30.5	-1.1	-1.2	
102:45:08	44			-0.8		
102:45:17	53	40	12.2	-0.8		
102:45:21	57	30	9.1	-0.8	-0.8	
102:45:31	67 ^a		1.7			-0.8
102:45:40	76	5.6	1.7		-0.4	0.0
102:45:43	79	0	0.0		-0.57	-0.57

^aNot reported by the crew.

In order to make descent data match what the photographs of the landing site suggest, the following scenario emerges: Assuming that between the heights 30.5 m (=100 ft) and 1.7 m (=5.6 ft, the height of the LSSP) the LM descends with the, up to that point average, sink rate of $v_x = -0.8$ m·s⁻¹, then it reaches the LSSP height at 67 s (GET 102:45:31). Up to that point, this fixed sink rate descent follows [28] if one has nulled horizontal velocity. However, because the horizontal velocity turns out to be greater than the maximal safe velocity of 1.2 m·s⁻¹(=4 ft/s, presumably

in -Y direction) the crew stops the descent and puts the LM to hover mode. By changing the pitch to 5° the crew begins to decrease horizontal velocity, and when it drops to safe values, the crew initiates landing. While this scenario fits the altitude data and the photographs of the landing area, it also suggests that the “Contact Light” in the cockpit should have come on at the beginning of the ten-second hover, when the -Y/Left LSSP first touched the ground. From Fig. 8 it is clear that -Y/Left LSSP was not in constant contact with the ground so the “Contact Light” may have turned off before coming on again few seconds later, and the crew ignored to report it: It is interesting that even the NASA web site [27] documented a disagreement between the crew whether the “Contact Light” was on, or not.

There are at least two problems with the story so far:

1. If an operating rocket engine passed above the drag mark, it should have been completely erased. Therefore the drag mark by -Y[Left] LSSP before the nozzle should not exist. Yet, it is there, and only central section directly under the nozzle is erased. This suggests that, for some reason, the rocket engine was not working until the LM reached its vertical landing position, then it was turned on during the landing.
2. Final resting position of the -Z[Aft] LSSP is radially outwards, that is, perpendicular to the horizontal direction of motion at touchdown. This together with the mound under the -Z[Aft] footpad suggests that at touchdown the LM was moving in the +Z direction, rather than in the -Y.

On the contrary, instrumental data suggests incline in Z-direction (where +Z is higher than -Z): Could have somebody decided to rake a mound of sand under the +Z footpad, so to balance the LM?

2.1.4. Blanchard's Findings

Blanchard in their investigation examined landing of the Lunar Module prototype in simulated lunar conditions on Earth. Of 21 investigated landings 11 were of, so called, 2-2 type (cases 1 through 7, and 18 through 21), while the rest was of 1-2-1 type (cases 8 through 17). The Blanchard findings can be summarized as follows:

- Friction between the footpads and the landing surface is mostly avoided by constraining the footpads not to move after the impact, while the change in the center-of-mass height in the impact contributes to kinetic energy of the impact. Kinetic energy of impact KE relates to

the total deformation energy DE, as

$$0.9 \cdot DE \leq KE \leq DE, \quad (2.3)$$

with potential energy of settling PE taking the rest in the absence of friction, $PE + KE \approx DE$.

- Kinetic energy is mostly (90% - 95%) dissipated in the primary struts, and mildly (5% - 10%) dissipated in the secondary struts.
- In the absence of horizontal motion, in landing on flat surface all gears approximately absorb same amount of energy.
- Horizontal kinetic energy is mostly dissipated in compression of one (in 1-2-1 landing), or two (in 2-2 landing) primary struts. However, the secondary struts pattern of compression and elongation is consistent with the direction of the horizontal motion, where within one group (of two secondary struts holding one primary strut) one strut is mostly compressed and the other elongated. Following compression of some, all secondary struts eventually undergo some elongation as the lunar module settles on the surface.

In all the landings considered by Blanchard the sink rate of the LM prototype was substantial in that the primary struts were always deployed.

2.2. Discussion and Conclusions

From the tabulated deformation energies it is obvious that only 50% of impact KE is absorbed in the deformation of landing gear. Of the absorbed energy, the -Z landing gear absorbed as much as all the other gears together. The LM was moving in -Y direction when it landed, so according to Blanchard, the -Y gear should have absorbed most of the impact energy (followed by +Y, and then much smaller +Z[Front] and -Z[Aft], see case #16), particularly because (as the LSSP drag marks suggest) the surface was slightly elevated along the Y-axis compared to the Z-axis.

We try to determine where the rest of the impact energy went. In the absence of primary strut compression the energy conservation reads,

$$KE + PE \approx \Phi_2 + E, \quad (2.4)$$

where PE is the change in potential energy associated with the deformation of landing gear, while

E represents the energy sink, for which there are two possible mechanisms: the friction between the footpads and the surface, and the soil penetration:

- *Friction:*

Here, $E \equiv E_{fr} \approx \text{KE} - \Phi_2 = \int ds F_{fr} = 1.3 \text{ kJ}$, or approximately $E_{fr} \approx \text{KE}_y$. Using the sand friction coefficient $\mu = 0.4$, this gives the distance of $d \approx 0.3 \text{ m}$ each footpad would travel on average. For comparison Rogers reports that post-flight simulation predicted travel distances of 0.45-0.56 m (=18-22 inch). There is a number of problems with this interpretation:

1. The duration of braking is approximately 1 second and this would be noticed by the crew.
2. The photographs of the footpads do not support any longer travel distances. Consider that the footpads are shrink wrapped (so the friction between the soil and the wrapping is definitely greater than the friction between the footpad and the wrapping), any dragging of the footpads against the surface would leave at least one of the two marks - either there would be a tearing and tensioning of the wrapping at the location where it is pulled under the footpad, or there would be deformation of the wrapping at the location where the wrapping would exit from under the footpad. Again, the photographs show pristine and undisturbed wrapping on all footpads and so do not support sliding in the sand as a way of dissipating the horizontal kinetic energy.

- *Lunar Soil Penetration*

We assume that the footpad is like spherical cap. We find that the radius of the sphere is $r = 1.5 \text{ m}$, while the depth of the cap is $d = 7 \text{ cm}$. Then, as the footpad penetrates the lunar sand by depth x_2 , its contact surface S_{foot} varies as

$$S_{foot} = 2 \pi r x_2. \quad (2.5)$$

The resistance of the Moon surface to penetration can then be described

$$R_{moon} = 4 \times P_{moon} \cdot S_{foot} = 8 \pi r P_{moon} x_2, \quad (2.6)$$

where we assume that the resistance pressure $P_{moon} \approx 34 \text{ kPa}$ (=5 psi after Surveyor data).

This allows us to express $R_{moon} = k_{moon} \cdot x_2$, where

$$k_{moon} = 1.3 \cdot 10^6 \text{ N/m}, \text{ and } \omega = \sqrt{\frac{k}{m^{LM}}} \approx 14 \text{ s}^{-1}. \quad (2.7)$$

Assuming that the vertical kinetic energy is approximately dissipated in the soil penetration yields for the penetration distance

$$x' \approx \frac{v_x}{\omega} = 4.8 \text{ cm}, \quad (2.8)$$

where for comparison the footpads are 7 cm deep.

Again, the photographs of the footpads do not support either of them being half sunk in the sand, so we assume hard-surface limit for the lunar soil.

We conclude that in the absence of penetration the impact energy must have been dissipated in the friction between the footpads and the surface.

However, the friction force is too low in magnitude to provide sufficient dissipation over distances much shorter than the footpad diameter. This is where one sees that in the absence of primary strut compression the reaction force of the Moon was $R_{moon} \simeq g m^{LM}$, so the friction force $\mu R_{moon} \simeq \mu g m^{LM} \sim 4 \text{ kN}$ with $\mu \simeq 0.4$. Conversely, were the primary struts shortened, this would (among other things) indicate that the Moon reaction force is $R_{moon} \simeq 4 F_{PS} \sim 80 \text{ kN}$, where the primary strut compression load is $F_{PS} = 20 \text{ kN}$ for displacements under 25.4 cm (=10 inch).

2.3. Discussion and Conclusions

Overall, the photographs suggest that the footpads traveled much smaller distances than anticipated from energy conservation, while the Rogers' secondary strut strokes magnitudes and directions fail to support the notion that the LM was landing with horizontal velocity in -Y direction. For that reason we consider a possibility that the entire scene was staged, where the LM (or its replica) of unknown mass m_x is lowered until its footpads touch the surface, then released to settle. In the absence of motion, the conservation of energy reads

$$\Delta\text{PE}(\Delta s) = \Phi_2(\Delta s) + E_{fr}(\Delta s), \quad (2.9)$$

where ΔPE is the change in potential energy of the LM as it settles against a hard surface after being released at zero height and with zero velocity somewhere on Earth. Without the access to

NASA computer program for calculation of landing dynamics, our analysis is quite rough:

Rogers data gives for the average secondary strut stroke per landing gear $\Delta s = 5$ cm. We assume that each footpad travels the same distance Δs across the surface, and that the center of mass of the LM drops down by the same distance Δs , all in the Earth gravity of $g_E = 9.81 \text{ m}\cdot\text{s}^{-2}$. Eq. (2.9) thus becomes,

$$m_x g_E \Delta s = \Phi_2 + m_x g_E \mu \Delta s. \quad (2.10)$$

We solve this for m_x and find $m_x \approx 4,200$ kg. For comparison, the dry mass of the LM is $m_{dry} \sim 4,900$ kg.

We conclude that the secondary struts deformation is consistent with the staging of the landing on Earth. In the context of landing being staged on Earth it is easy to see why the -Z[Aft] landing gear is elongated the most: during the staging somebody noticed that the footpad is in the air when the other three footpads touched the ground, so they put a mound of sand under the footpad to balance it. When the LM was released to settle the landing gear slid off the mound while slightly deforming it giving the appearance that the mound resulted from dragging the footpad in the sand (even though it was the lowest point on the surface and the footpad touched it the last).

In addition, the trace the LSSP makes in AS11-40-5921 is puzzling because under the rocket engine nozzle a section of the trail is still visible. The interaction between the rocket engine and the lunar soil would determine the condition of two elements of the LM undercarriage: the radiation shield (a few-microns thick gold foil around the bottom of the Descent Stage), and the protective shrink wrapping (Kapton and mylar) of the landing gear. In the literature there are two descriptions of the interactions. The images of the Apollo 11 landing site, and blast zone in particular, are consistent with the *bearing failure* theory that was developed around the time of the Apollo programme. According to this theory, lunar sand flows down and perpendicularly outwards from the rocket jet to make a wide and shallow indentation in the sand, where the sand flow never reaches the undercarriage. The pristine Apollo 11 undercarriage and the miniscule congregation of dust on the landing gear and inside the footpads all support the theory, e.g., see images AS11-40-5921 [20, 24] or AS11-40-5927 [20, 29]. However, Metzger *et al.* [30] have shown that this theory is inaccurate. They found that when operated close to a sandy surface, the rocket jet digs a hole of comparable diameter along the edge of which the sand flows tangentially upwards. Were this true for the Apollo 11 landing, the amount of sand excavated from the hole at high velocity would have sand blasted the undercarriage clean of any shrink wrapping and leave visible abrasion marks.

Obviously, if the rocket engine were operating there would be no traces in the sand anywhere near the nozzle. Again, what we see is consistent with the landing being staged on Earth in which the LM rocket engine may have been running for a second or two.

We use these conclusions to comment on the behavior of the Descent Stage of the Apollo 17 during lift-off. As Rogers' data suggests the primary struts are quite stiff requiring forces greater than 80 kN to become shorter, but the secondary struts are not. For that reason, the DS should have flexed during the lift-off under the combination of rocket engine thrust F_{th} and the explosion force F_a , both of which are greater than the weight of the dry DS ($F_a/F_{th} \sim 2$, and $F_{th}/(m_d^{DS} g) \gtrsim 3$). On the contrary, the DS was so rigid during the lift-off that we used the top of the primary strut as one of the reference points for measuring distances. Conspicuous absence of any DS motion suggests that we are looking at a scaled-down lift-off featuring detailed models. We further develop this idea in the next section.

2.4. Tables and Figures

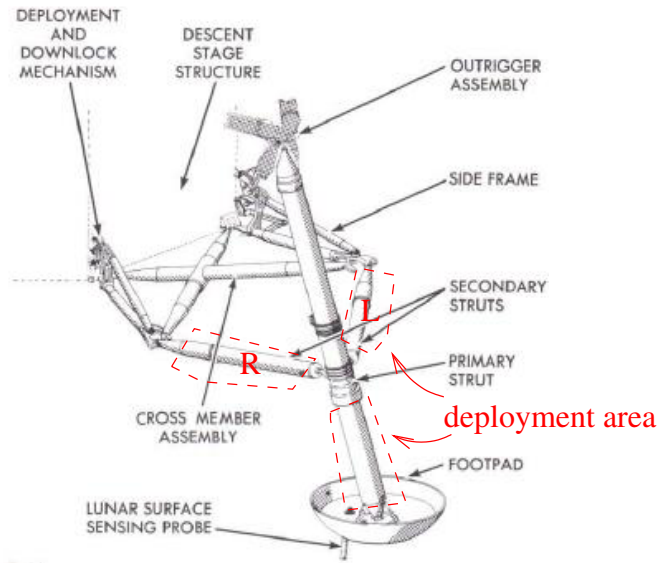


FIG. 6: Landing gear assembly features impact energy absorbing primary strut and two supporting (Left and Right) secondary struts. [15] While the primary strut may only shorten under compression, the secondary struts may shorten under compression or elongate under tension. Their deployment areas are marked in red.

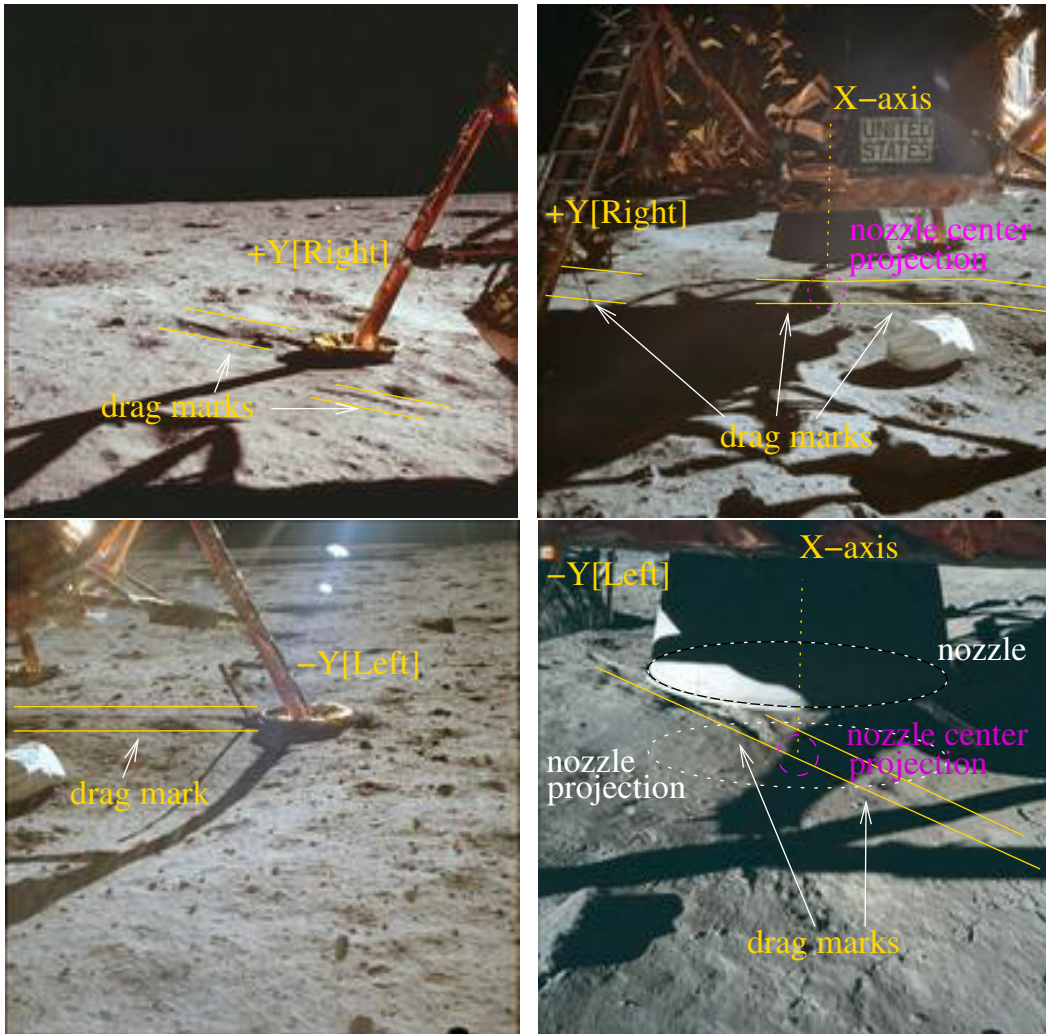


FIG. 7: The photograph AS11-40-5858 (top left) shows +Y[Right] gear and its Lunar Surface Sensing Probe (LSSP) drag mark. The drag mark in front of it, as suggested by the photograph AS11-40-5864 (top right) may have been made by the -Y[Left] LSSP. Multiple drag marks made by the -Y[Left] LSSP can be seen on the photograph AS11-40-5865 (bottom left) and on AS11-40-5921 (bottom right). Detailed view in the photograph AS11-39-5821 (bottom right) suggests that only a section of the -Y[Left] LSSP drag mark directly under the nozzle has been erased.

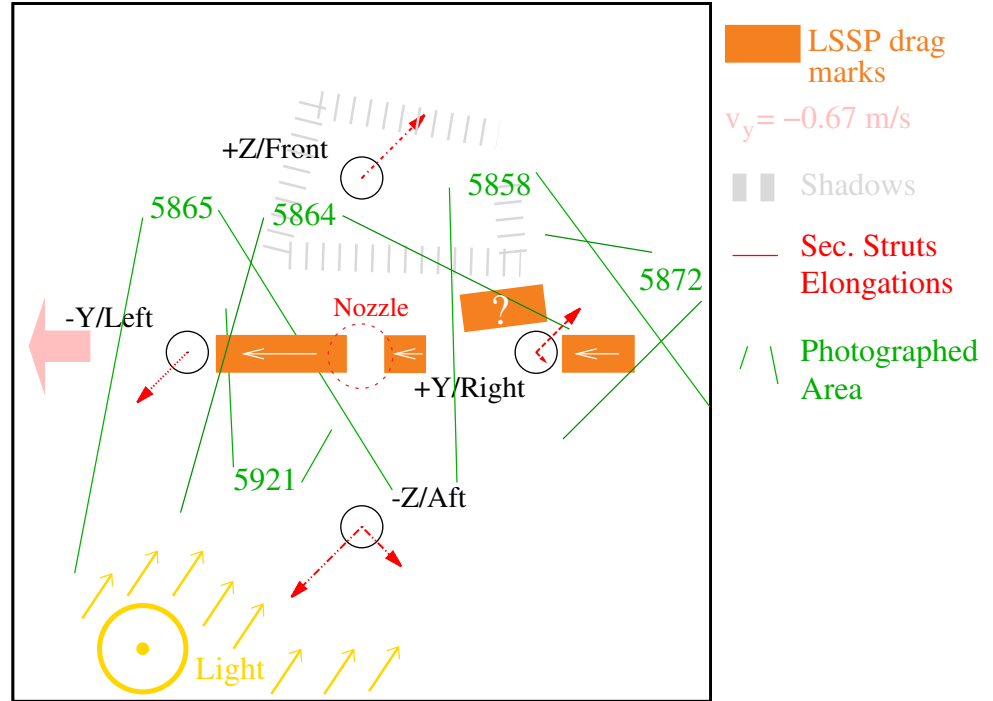


FIG. 8: Not-to-scale sketch of the Apollo 11 Lunar Module landing that summarizes Rogers' data (direction and magnitude of horizontal velocity at touchdown, elongation of left and right secondary struts of each landing gear) and the LSSP drag marks from Fig. 7 with the numbers of reference photographs used in their reconstruction. The photograph AS11-40-5872 [20, 31] suggests that the drag mark above the +Y[Right] footpad (indicated with white '?' on orange background) is directed toward the two drag marks made by the -Y[Left] LSSP.

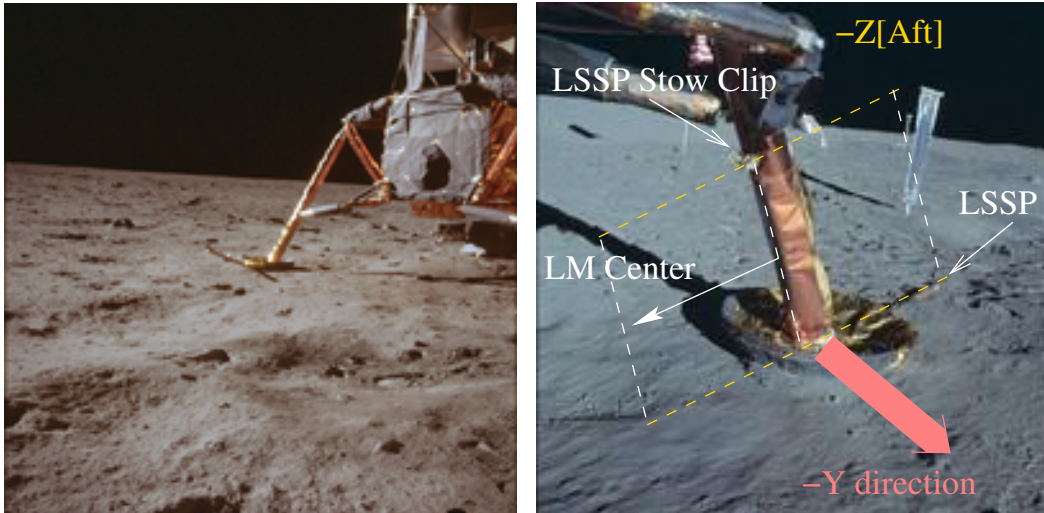


FIG. 9: In the photographs of the $-Z[Aft]$ landing gear AS11-40-5914 (Left panel) and AS11-40-5920 (Right panel) firstly, the Lunar Surface Sensing Probe (LSSP) failed to make any drag marks beyond its length unlike the landing gears $\pm Y$'s LSSPs; and secondly, its final resting position is approximately radially opposite the LM center rather than opposite the horizontal direction of motion at touchdown in $-Y$ direction.

3. ALSO SPRACH ZARATHUSTRA

We return to the Apollo 17 lift-off video recording [10] and analyze it in greater detail following the findings of last two sections. For the purposes of our analysis we convert the video clip to a set of images at rate $r = 25$ frames-per-second (fps) [48]. We firstly analyze the images $[681 : 901]_{25}$ featuring stationary Lunar Module (LM) prior to the lift-off. Then we examine size and illuminance of the ascending LM in the images $[981 : 1012]_{25}$.

3.1. Film Stock

Method: We examine frames $[681 : 901]_{25}$ using the software package GIMP [14], at various brightness and contrast settings.

Findings: In the frames $[681 : 685]_{25}$ under the extreme settings of 127 for brightness, and 127 for contrast we find identical artifacts that strongly resemble an edge of film stock. We show the frame 681_{25} in Fig.10 in which the artifact stretching horizontally across the image is obvious. Presence of the film stock is surprising, considering that NASA claims that this video was recorded by a television camera. [3]

3.2. Flicker

Following an examination of video recording with the software package `ffmpeg`, it transpires that it was recorded at the 25 fps. During the watching the video recording appears to be flickering.

Method: For each image in the sequence $[681 : 901]_{25}$ we determine the average values for red, green and blue channel. [32] From the averages we create three 221-samples long time series $\{R_{680+i}, G_{680+i}, B_{680+i}\}_{i=1,221}$. We regularize each series with its total average $\bar{R}, \bar{G}, \bar{B}$, so $a_i = A_i/\bar{A} - 1$, for $\{a, A\} = \{\{r, R\}, \{g, G\}, \{b, B\}\}$. We then split regularized time series to 128-samples long sequences, which we Fourier Transform, and then average so found modulation depths.

Findings: As can be seen from Fig.11 there is light flicker in the video recording, which frequencies are 5 Hz and 10 Hz, where the red and green peaks are stronger at 5 Hz than at 10 Hz, while the blue is the opposite.

Discussion: As is known, one way of creating 5 Hz flicker consists of using a film camera that records at 25 fps, while the illumination is provided by incandescent lamps (have strong red component) operating at 60 Hz, so its light output is modulated at 120 Hz, which is twice the mains frequency. More precisely, 120 Hz signal when sampled at 25 Hz becomes 5 Hz because of

aliasing. Because of the non-linear characteristic of incandescent lamps, where their light output is proportional to input power and the temperature of the filament, the light may contain second and higher harmonics, hence the 10 Hz peak. The modulation depth of the recorded light is in the range $\sim 1\%$ (blue) to $\sim 3\%$ (red), which is lower than the actual modulation depth of the incandescent lamps ($\gtrsim 10\%$) because the camera exposure time acts as an integrator (low-pass filter).

We isolate the 5 Hz changes in the lighting patterns using GIMP [14], where we set brightness to 50 and contrast to 127. In Fig. 12 we show a 6-frame sequence $[681 : 685]_{25}$, and there the lighting pattern can be recognized (*i*), in the lower right corner with respect to the Lunar Module (ground on the right from the LM); and (*ii*), on the hill on the right (which is presumable far) behind the LM. The two lighting patterns are consistent with the LM being side- and back- illuminated with incandescent lamps in-phase (from the same source). However, that the illumination of the entire hill (presumably Camelot) is uniformly modulated suggests that the hill is a two-dimensional image of a geographical feature close to the LM, rather than a spatially extended feature stretching far behind the LM.

3.3. Space Rocket or Space Elevator?

We look at the images $[981 : 1012]_{25}$ depicting the last 1.3 s of the ascent, after which the camera view changes to inside view. In Tbl. IV we list the positions of bottom left corner of the LMAS in each image, where the x direction is horizontal, while y direction is vertical. We note that the camera almost perfectly follows the LMAS.

It has been proposed many times in public media that the video features the LMAS replica being pulled up in, what we call, the space elevator, rather than the real LMAS being propelled by its own space rocket. The two propulsion mechanisms, space rocket vs. space elevator, have different center-of-pressure: For rocket powered LMAS, the center-of-pressure is the exit of combustion chamber (at the bottom if we neglect the nozzle), while for hoisted replica, the center-of-pressure is the attachment point to the elevator (top of the object). It is important to recognize that two propulsions react differently to perturbations, where the perturbations are most pronounced opposite the center-of-pressure. The real LMAS is marginally stable with respect to changes in roll or pitch angles, so the real LMAS moving upwards may also drift sideways.

The replica pulled up can be described as a simple gravity pendulum of arm length l_{CM} , in an accelerating space elevator with the acceleration $a_e \approx \text{const}$. It performs harmonic motion with the frequency of small oscillations $\omega = \sqrt{(a_e + g)/l_{CM}}$.

We depict the distinction between two propulsion mechanisms in Fig. 13.

The video recording features few swings of the bottom of the object, of which one half-period can be clearly identified in images [994 : 997]₂₅. Its duration is $\sim 3/25 = 0.12$ s, while its appearance suggests under-damped motion of period,

$$T_{v:a17} \gtrsim 0.3 \text{ s}, \quad (3.1)$$

and frequency $f_{v:a17} \sim 4$ Hz. A true-to-life replica being hoisted up somewhere on the Earth would have oscillated with a period

$$T_{AS} > 2\pi \sqrt{\frac{l_{CM}}{g_{Earth}}} = 3.1 \text{ s}, \quad (3.2)$$

where $l_{CM} = 2.4$ m is the center-of-mass distance from the center-of-pressure. We find $T_{AS} \gg T_{v:a17}$, so the featured object is not true-to-life replica. However, if this were a 1:48 scale model, then its period would be $T_{AS} \sim 2.4/\sqrt{48} \sim 0.45$ s, which is of the same order of magnitude as $T_{v:a17}$.

3.4. Heading for the Light

One may argue that the object motion cannot be detected with certainty because of the poor resolution of the images. Were we able to see specular reflection of the Sun from the object surface this would have increased our chances to detect micro-motion - we would just have to look for modulations in magnitude of the specular reflection beyond the observed 5 and 10 Hz, provided they not saturate the camera. However, we find no evidence of specular reflection just from the geometry of the scene: the Sun is at least 50° above horizon behind the camera, while for the duration of video recording analyzed here the object moves from 6° to 12° above horizon and does not approach to the Sun's angle.

Rather, we notice that if the video recording is from the Moon then the light comes from the Sun at infinity, so its angle with respect to the object is fixed during lift-off. Then, the average illuminance of the LMAS should be constant for as long as the angle between the LMAS and the Sun, and the angle between the camera and the LMAS are sufficiently different so we do not have specular reflection. Conversely, if the scene is staged scaled down, then the lighting is provided by arrangement of near-by lamps, and the camera might be able to capture systematic changes in illuminance if the object as it ascends approaches to the stage lighting.

We determine the average illuminance of the object as follows. For each image in the sequence [981 : 1012]₂₅ we isolate the segments 61 pixels wide and 46 pixels high, which lower left corner are given in Tbl.IV. In Fig. 14 we combine all analyzed image segments in one composite image. The segments feature the AS, black background and some reflections from the dust. We introduce threshold λ^a , $a = R, G, B$, and in each image segment determine mean pixel value above the threshold λ^a ,

$$\bar{c}^{a,k}(\lambda^a) = \frac{1}{\sum_{i,j} \mathcal{H}(c_{i,j}^{a,k} - \lambda^a)} \sum_{i,j} \mathcal{H}(c_{i,j}^{a,k} - \lambda^a) \cdot c_{i,j}^{a,k}, \quad (3.3)$$

where $k = 981 \dots 1012$, while Heaviside function is $\mathcal{H}(x) = 1$ for $x > 0$, and 0 otherwise. In Fig. 15 (top panel) we can see that the average pixel value $\bar{c}^{a,k}$ for $\lambda^a = 50$, $a = R, G, B$, increases with image number, that is, as the object gains height.

One possible explanation of this effect is given in Fig. 15 (bottom panel). The object illuminance is a function of the light source altitude θ , as

$$l_\theta = \frac{S \cos \theta}{r_\theta^2}. \quad (3.4)$$

We find how does the relative illuminance changes between two positions, the initial 0 and some later 1, if we assume that the source of light is at distance b from the line along which the object ascends. Then the ratio of illuminances between two positions is,

$$\frac{l_{\theta_1}}{l_{\theta_0}} = \frac{\cos^3 \theta_1}{\cos^3 \theta_0} \simeq 1 - 3 \tan \theta_0 \cdot (\theta_1 - \theta_0) + \dots \quad (3.5)$$

We find $\Delta x \cdot \cos \theta_0 = b / \cos \theta_0 \cdot \Delta \theta$, where $\Delta \theta = \theta_1 - \theta_0 \leq 0$ and $\Delta x = x_1 - x_0 \leq 0$. We know that the object moves so $x(t) = \frac{1}{2} \hat{a}_1 t^2 + \hat{v}_1 t + \hat{x}_1$, so $-\Delta x = \frac{1}{2} \hat{a}_1 \Delta t^2 + (\hat{a}_1 t_0 + \hat{v}_1) \Delta t \propto \Delta t^2 + 2(\hat{a}_1 t_0 + \hat{v}_1) / \hat{a}_1 \Delta t$. With the timing information from the image sequence, $t_0 = (981 - 902) / 25 = 3.2$ s, we find $2(\hat{v}_1 + \hat{a}_1 t_0) / \hat{a}_1 \simeq 7.4$ s, so the theoretical prediction for the change in illumination is,

$$\frac{l_{R,G,B}(\Delta t)}{l_{R,G,B}(t_0)} = k_2 (\Delta t^2 + 7.4 \text{ s} \cdot \Delta t) + k_{R,G,B}. \quad (3.6)$$

From the pixel data we find $k_2 \simeq 0.0092 \text{ s}^{-2}$, and $k_{R,G,B} = 0.98$. In Fig. 15 (top panel) we compare the average pixel channels to the best-fit models (3.6), and find an excellent agreement. An upper

limit on the distance b between the light source and the AS trajectory thus reads,

$$b = \frac{3 \hat{a}_1 \sin(2\theta_0)}{4 k_2} \leq \frac{3 \cdot \hat{a}_1}{4 k_2} \sim 160 \text{ m.} \quad (3.7)$$

For comparison, the distance between the camera and the object is $b' = 120 \text{ m}$.

Obviously, if $b \sim b'$ then the lighting for the scene could not have been provided by the Sun. We thus scale all distances down to 1:48, which we came to expect from the micro-motion of the Lunar Module Ascent Stage replica to find,

$$b \simeq 3.5 \text{ m, and } b' \simeq 2.5 \text{ m.} \quad (3.8)$$

3.5. Baby, you are firework!

If the entire lift-off was staged on the Earth, using 1:48 replica then the question is how it was performed.

Firstly, from the flicker caught on the video recording we conclude that the time scale was not changed.

Secondly, in order for the replica on the Earth to achieve constant acceleration, a system of cables and pulleys has to be in place with the LMAS being on one end of the cable, and some extra mass $M > m^{LM}$ on the other end. Assuming single pulley with a cable, and two masses on each side of the cable, the acceleration of the system is

$$a \simeq \frac{(M - m^{LM}) \cdot g_{Earth} - F_{fr}}{M + m^{LM} + \frac{I_p}{R^2}}, \quad (3.9)$$

where I_p is the moment of inertia of the pulley and R is the radius at which the cable interacts with pulley, while F_{fr} is the friction force between the moving and the stationery parts of the contraption.

Assuming no friction and massless pulley, the target acceleration of the replica is $a_T \sim 2 \text{ m} \cdot \text{s}^{-2}/50 = 0.04 \text{ m} \cdot \text{s}^{-2}$. As $a_T/g_{Earth} \simeq 0.004 \ll 1$, we know $M = m^{LM} + \Delta m$ with $\Delta m \ll m^{LM}$ so $\Delta m/(2m^{LM}) \approx a_T/g_{Earth}$. We assume replica of mass $m^{LM} = 0.5 \text{ kg}$ so the extra mass is $\Delta m \simeq 4 \text{ g}$.

The friction force will make it difficult for two masses to start moving with the target acceleration. This is because the friction force will start as static F_{fr}^s before masses start to move, then become dynamic F_{fr}^d with their motion, where $F_{fr}^d < \Delta m \cdot g_{Earth} < F_{fr}^s$. For that reason, Δm has

to be chosen so that net force that includes F_{fr}^d produces target acceleration. However, for the two masses to start moving, they have to get a push that will help them overcome static friction F_{fr}^s . In popular vernacular the hypothetical source of that push is known as the *Chinese Firecracker theory*, which fits perfectly our findings from Section 1.

Our final remark is that the hoisted replica can still be seriously perturbed by a firework exploding under its rear. As this is not shown on the video recording, we surmise that the replica could only move along a railing.

3.6. Conclusions

Analysis of the entire lift-off strongly suggests that the scene features a smaller scale replica, say 1:48, being pulled up on a stage of size ~ 4 m across. In this scaled setup, fireworks are required for the replica to overcome the static friction and to start moving with target acceleration. The stage lighting appears to be driven by 60 Hz VAC, suggesting that the studio was in the United States. That the incandescent studio lights appear to be flickering at 5 Hz, together with the artefacts on the images similar to the edge of film stock, suggest that the entire scene is recorded with a film camera, which for some reason operated at 25 fps (European standard) and not at 24 or 30 fps (the USA standard).

3.7. Tables and Figures

Frame (s)	X (pixel)	Y (pixel)
984	204	175
985	204	175
986	204	175
987	204	175
988	204	175
989	204	175
990	205	175
991	205	177
992	205	177
993	205	176
994	205	176
995	203	175
996	204	174
997	205	174
998	205	173
999	205	174
1000	205	173
1001	205	173
1002	205	173
1003	205	173
1004	205	173
1005	205	173
1006	205	172
1007	205	172
1008	205	172
1009	205	171
1010	205	170
1011	205	170
1012	205	170

TABLE IV: X- and Y-pixel coordinates of the bottom left corner of the Lunar Module Ascent Stage in the images [984 : 1012]₂₅. Please note mild lateral oscillation in the frames [994 : 997]₂₅.

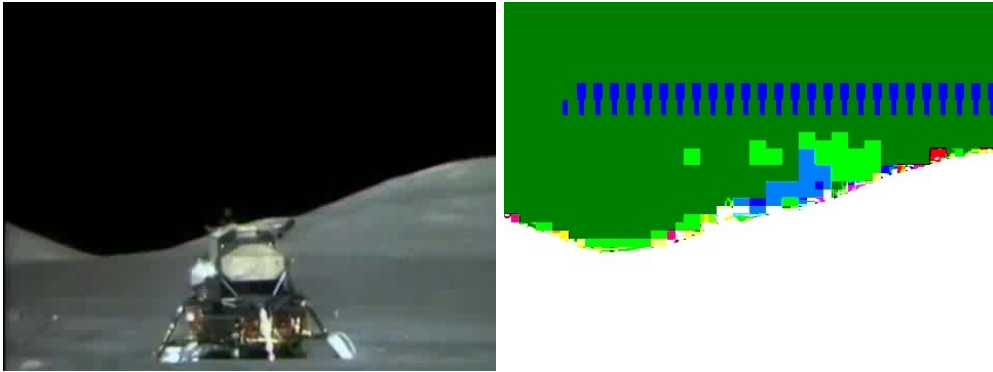


FIG. 10: The images $[681 : 685]_{25}$, with which the video-recording of liftoff actually starts (the preceding images showing the Apollo 17 mission patch), have identical artifact that strongly resembles an edge of film stock. The left panel shows the original image 681_{25} , while the right panel shows the same image manipulated with GIMP [14], to brightness 127 and contrast 127. The artifact is clearly visible across the top half of the image.

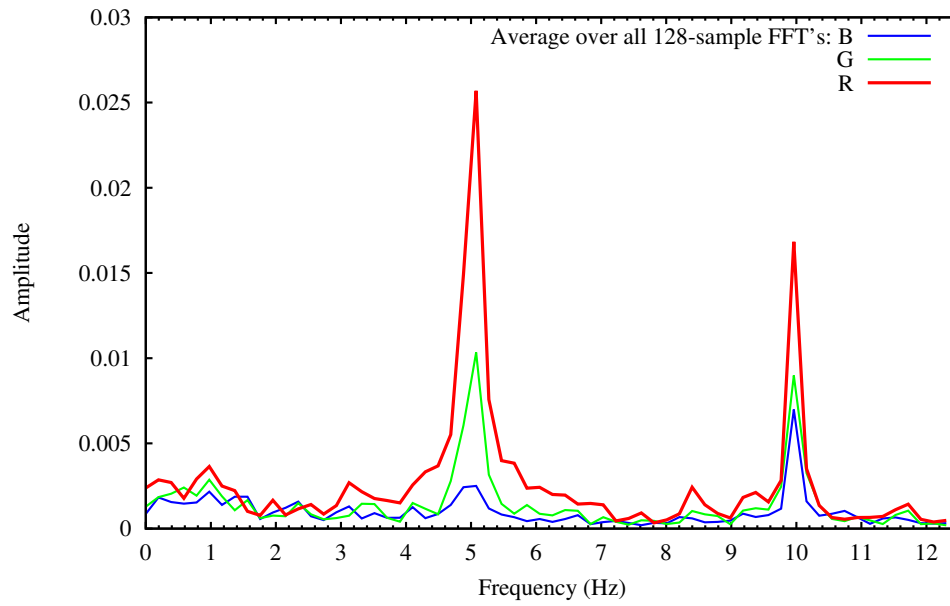


FIG. 11: Fourier Transform of the red, green and blue channels of images $[681 : 901]_{25}$ has strong 5 Hz and 10 Hz peaks. Hypothetical origins of the peaks are discussed in the text.

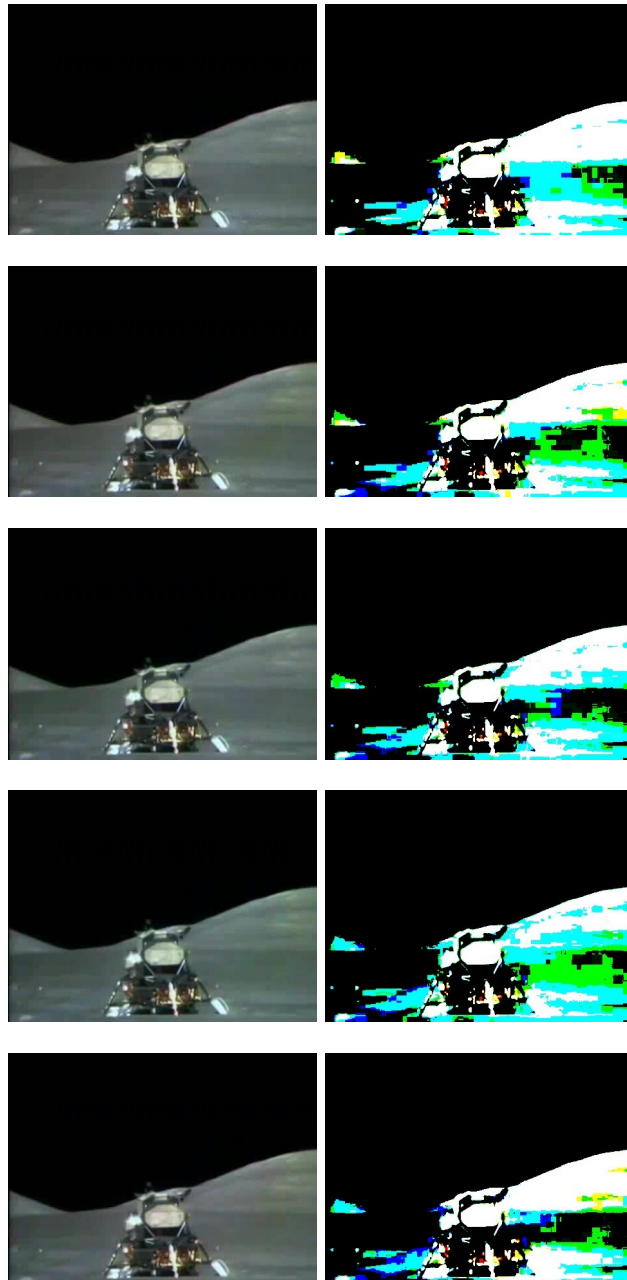


FIG. 12: 5 Hz pulsating light pattern in the images $[681 : 685]_{25}$ barely visible in the originals (left column) emerges after some post-processing (right column) in GIMP [14] (brightness 50 and contrast 127). The pattern comprises of periodic light fluctuations of two reflections on the ground on the right of the Lunar Module, and the brightness of the hill on the right (presumably Camelot, behind in the distance). The pattern repeats at 5 Hz (in sequences 5 images long, like the one shown) for the duration of pre-liftoff.

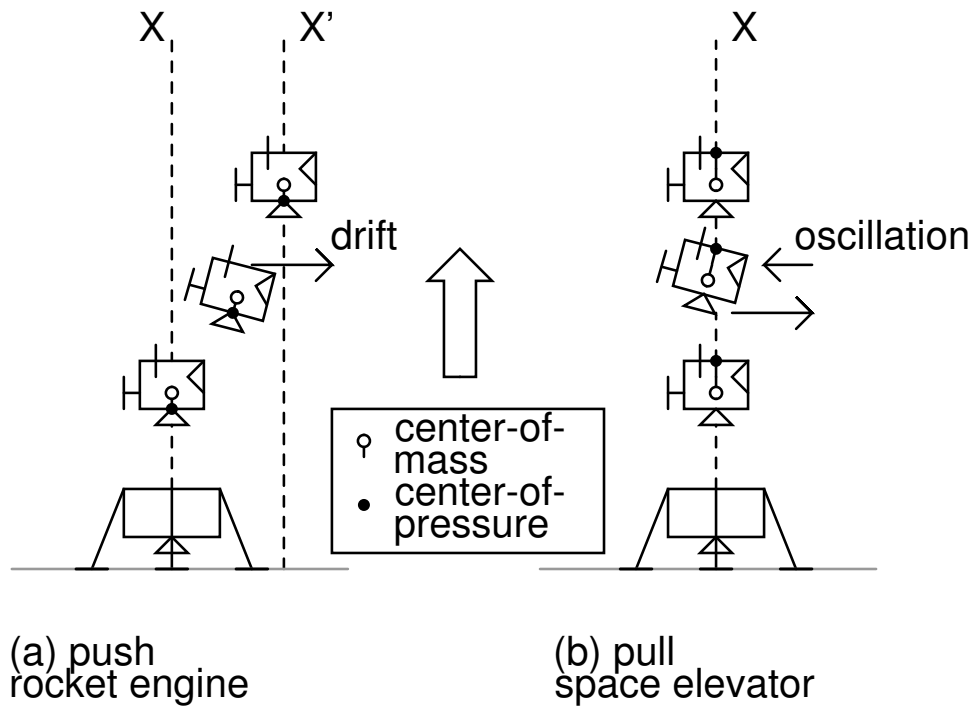


FIG. 13: Two propulsion mechanisms acting at the center-of-pressure on an object, *the push* by the rocket (left panel) and *the pull* by the rope where the center-of-pressure is constrained to vertical degree of freedom (right panel) are considered in the text. The perturbations to the motion manifest themselves differently. While under the push the object may drift sideways as the perturbations accumulate, under the pull the perturbations are self-rectifying all the while the center-of-pressure maintains its initial direction irrespective of perturbations.

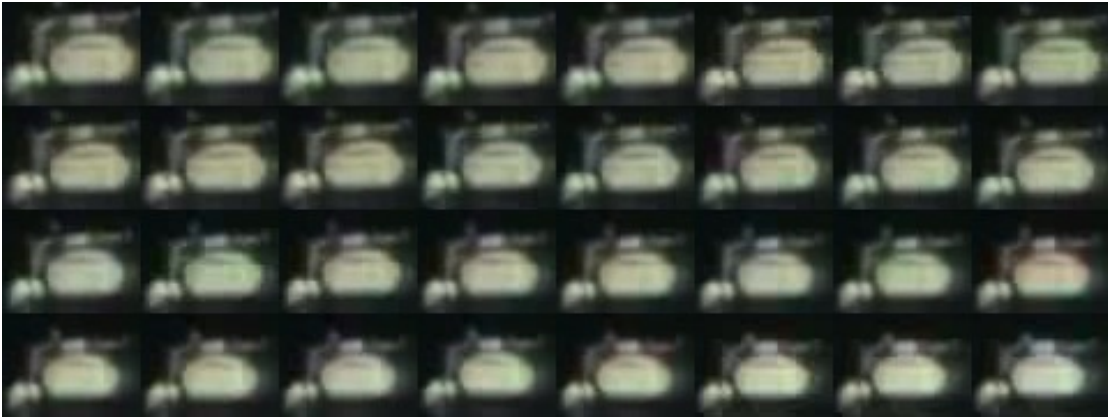


FIG. 14: 32 segments of size 61x46 pixels from the image sequence $[981 : 1012]_{25}$ of the liftoff. The segments are numbered from top to bottom, left to right, while the bottom left corner of the segment in the image is provided in Tbl.IV. Please observe that the Lunar Module Ascent Stage appears brighter as it climbs, while it size shrinks as the distance to the camera increases and because of the zoom-out, see discussion in the text.

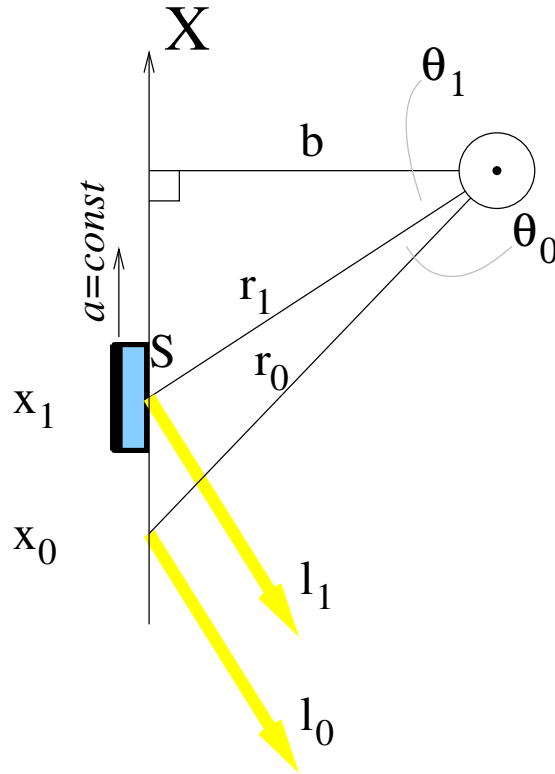
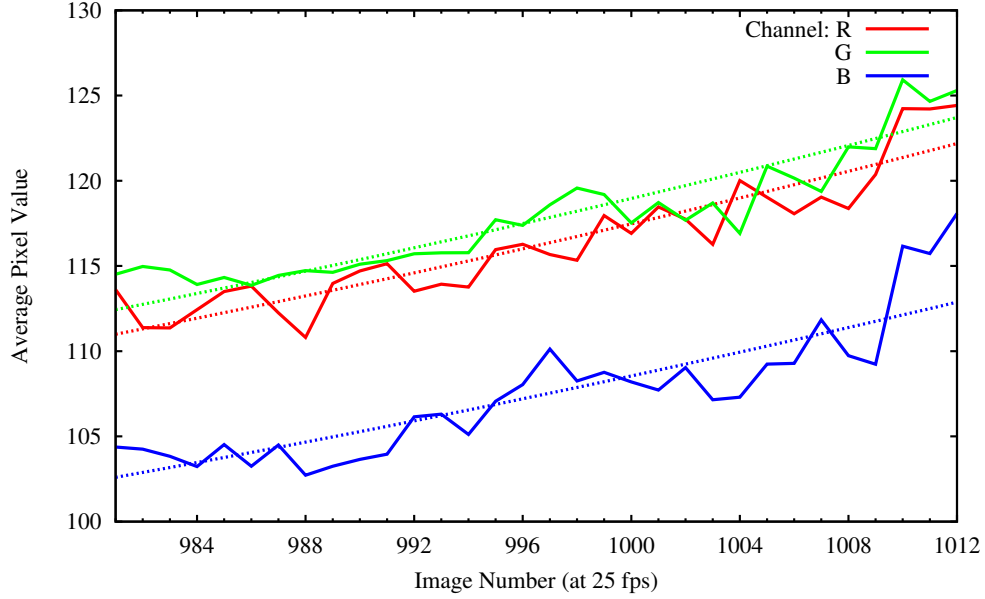


FIG. 15: (Top panel) The average pixel color channel values above cut-off $\lambda = 50$ increase as the Lunar Module Ascent Stage (LMAS) climbs. Were the LMAS illuminated by the Sun (for all practical purposes) at infinity, this should have been a constant as it represents an average illumination by the light source. (Bottom panel) The illumination of an ascending object (blue rectangle) may increase if the object is approaching the light source (astrological symbol for Sun), here at the distance b from the liftoff trajectory (coincide with the X-axis), see discussion in the text.

4. STANDING IN MOTION

The goal of this section is to examine 360° yaw performed during Undocking of Lunar Module from Command and Service Module, that occurred around Ground/Mission Elapsed Time (GET, or MET) 100 hr. As is known, the Apollo 11 has just passed behind the Moon on its last [circular] orbit before undocking, and two separate space crafts re-emerged. They would make one further lunar orbit, then the Lunar Module would enter its descent orbit. [33] In particular, we are interested in behavior of the lunar surface sensing probes (LSSP) in a sequence of photographs from Apollo 11 mission during the yaw. In illustration in Fig. 6 of the LM landing gear assembly, we show fully extended LSSP following the landing gear deployment early in the mission. In Fig. 16 we illustrate the LSSP in fully deployed position in absence of gravity. As is known, [7, 15] the LSSPs attached to each landing gear footpad, except the forward one, are the electromechanical devices. After deployment, the probes are extended so that the probe head is approximately 1.7 m below the footpad. When any probe touches the lunar surface, pressure on the probe head will complete (close) the circuit and activate “CONTACT” light on the LM control panel. The astronauts may then initiate the landing, e.g., by shutting down the LM descent engine.

The section organized as follows. In the second section we characterize the LSSP, and find its equilibrium position at rest in presence of gravity. In the third section we characterize the behavior of the LSSPs during a yaw with known rate. In the fourth section we use the NASA documentation to find the yaw rate during the 360° yaw. In the fifth section we compare calculated deflection of the LSSPs due to rotation, to the photographs of the LM performing the yaw, and draw conclusion.

4.1. LSSP Equilibrium Position at Rest with Hinge as Pivot

In NASA provided illustration in Fig. 16 (left panel), a LSSP comprises of three segments, the off-center segment a welded to the footpad, followed by the longer segment b , to which the longest segment c is attached at angle γ . Reading the distances directly from the illustration gives $a \simeq 0.2$ m, $b \simeq 0.3$ m, $c \simeq 1.5$ m, with $\gamma = 105^\circ$, which is for the quantitative discussion that follows misleading. Instead, we turn to the photograph AS11-44-6586 [20, 34] and find $a \simeq 0.18$ m, $b \simeq 0.35$ m, $c \simeq 1.25$ m, and most importantly $\gamma = 150^\circ$.

The fully deployed position was acquired at the start of Trans-lunar coast early in the mission. In this position the angle between a and b is maintained by a spring-loaded hinge (probably combined with a limiter), so that according to NASA illustrations, the segment c is parallel to the X-axis of

the LM. For the following discussion we measure all the positions with respect to the hinge, and all angles with respect to a line passing through the hinge parallel to the LM X-axis (vertical).

First, we find the deflection of the LSSP's free end assuming that the mass is distributed uniformly; that the gravity acts in the direction of the negative X-axis and that the hinge limits the motion of the beams to a plane (acts as a pivot point). Then, the LSSP will mildly flex inwards, toward the LM X-axis. The condition that the torque on the LSSP with respect to hinge is zero reads,

$$3b \sin \theta_g + c \sin(\pi - \gamma + \theta_{max}) = 0, \quad (4.1)$$

which solution is $\theta_{max} \simeq 164^\circ$. Radial displacement of the end of the LSSP compared to the radial projection of the pivot point (hinge) is then $\Delta y_0 \simeq -0.20$ m, that is, inwards.

Second, in the absence of gravity the spring in the hinge pushes θ to $\theta_0 = \gamma = 150^\circ$, so that the LSSP is parallel with the X-axis of the LM. One may notice that this is how the LSSPs are always illustrated in NASA documents. The limiter in the hinge thus allows only $\theta \geq \theta_0$, while gravity sets limit $\theta \leq \theta_{max}$.

Interestingly, we see that if the LM is suspended in presence of gravity, then combination of the hinge spring (pushing the LSSP outwards) and the gravity (pulling them inwards) puts the LSSP at an angle $\theta \in [\theta_0, \theta_{max}]$. This appears visually as the LSSP's being flexed mildly inwards toward the X-axis of the LM.

This being said, let us consider the photographs in which Collins using the 70 mm Hasselblad electric camera captured the 360° yaw (1 rev) of the LM following the undocking from the Command and Service Module (CSM). These photographs are AS11-44-6575 [20, 35], AS11-44-6576 [20, 36], AS11-44-6577 [20, 37], AS11-44-6578 [20, 38], AS11-44-6579 [20, 39], AS11-44-6580 [20, 40], AS11-44-6581 [20, 41], AS11-44-6582 [20, 42], AS11-44-6583 [20, 43], AS11-44-6584 [20, 44], AS11-44-6585 [20, 45] and AS11-44-6586 [20, 34]. From the account of the descent to lunar surface, it transpires that the LM yaw rate in the photographs was was 5 deg/s, which produced almost negligible centrifugal force that coincided with the action of the spring in the hinge.

We remark that flexibility in the hinge is necessary so that the LSSPs can move out of the way during landing, which is possible if the LM has some horizontal velocity at the moment when the LSSPs touch the lunar surface.

4.2. Results and Discussion

We analyze the photograph AS11-44-6586, in which we find that the angle between the segment b and X-axis is equal to $\theta_{a11} = 155^\circ$ for both left [Y-] and right [Y+] LSSP. Coincidentally, at this angle the end of the LSSPs are located almost-exactly under the hinge.

If we assume that NASA's reference drawings represent how the LSSPs were to be deployed, then the LSSPs being flexed mildly-inwards is consistent with the Lunar Module being suspended in the presence of gravity, rather than being weightless in a lunar circular orbit.

Conversely, as the exact specifications of the hinges have been long lost, it is possible that the limiters in the hinges were set to this particular position of 155° , so that during a straight down landing they would slide under the LM rather than ending poking out sideways (and so would have presented safety hazard for the crew moving around them, which they did in the end).

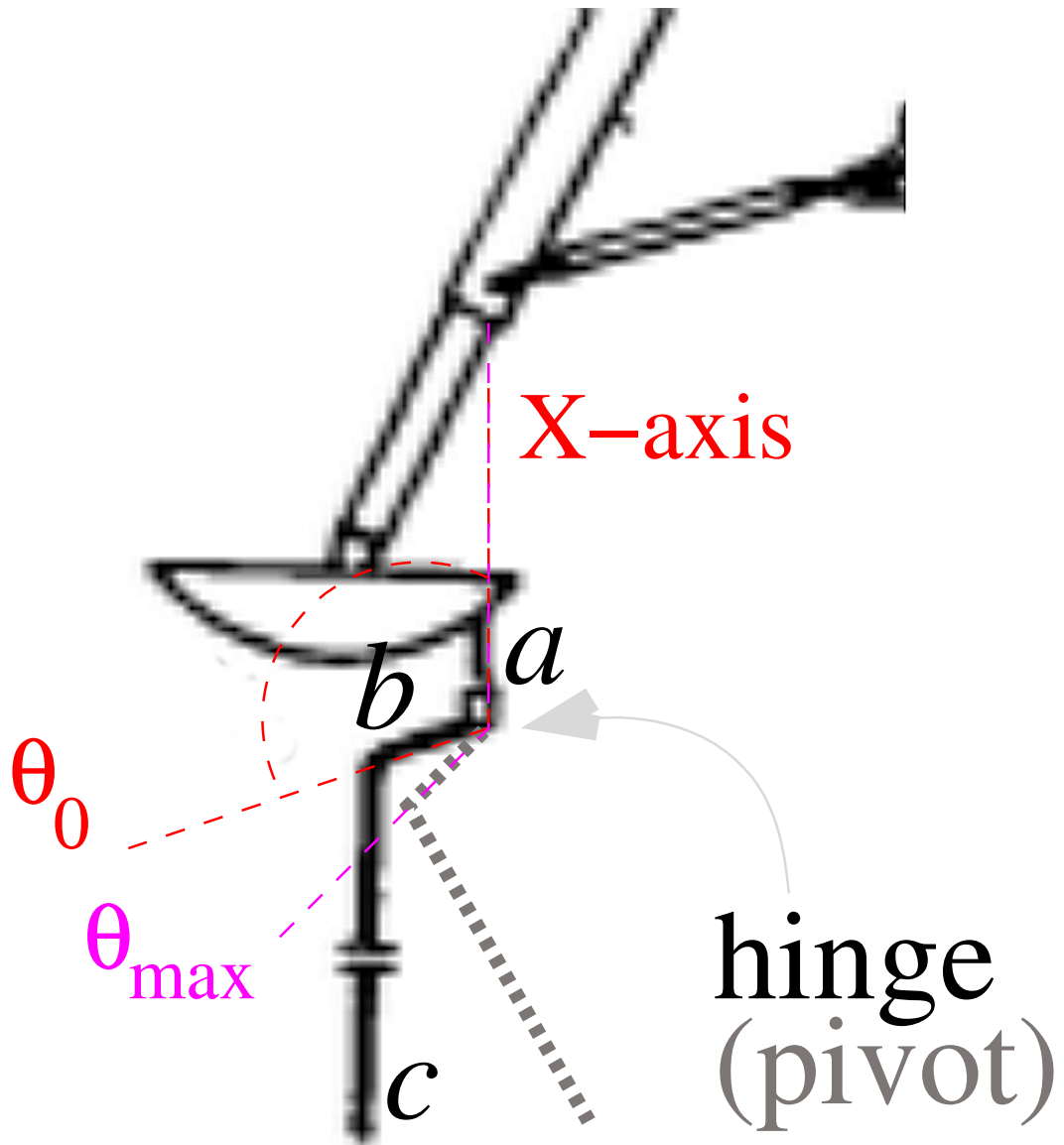


FIG. 16: Fully deployed Lunar Surface Sensing Probe (LSSP), [15] under weightless conditions features three segments, a , b and c . The segment a is fixed to the footpad, while segment b is attached to a through a spring-loaded hinge with a limiter. In this position b is at angle θ_0 from the X-axis (not a), so c is parallel to the X-axis of the Lunar Module. The original NASA drawing (shown here in fuzzy black lines) does not match the LM specifications for the LSSPs, cf. Fig. 17.

In the presence of gravity and having pivot point instead of hinge (no torque produced by the spring) puts b at an angle θ_{max} to X-axis (in thick dotted gray line).

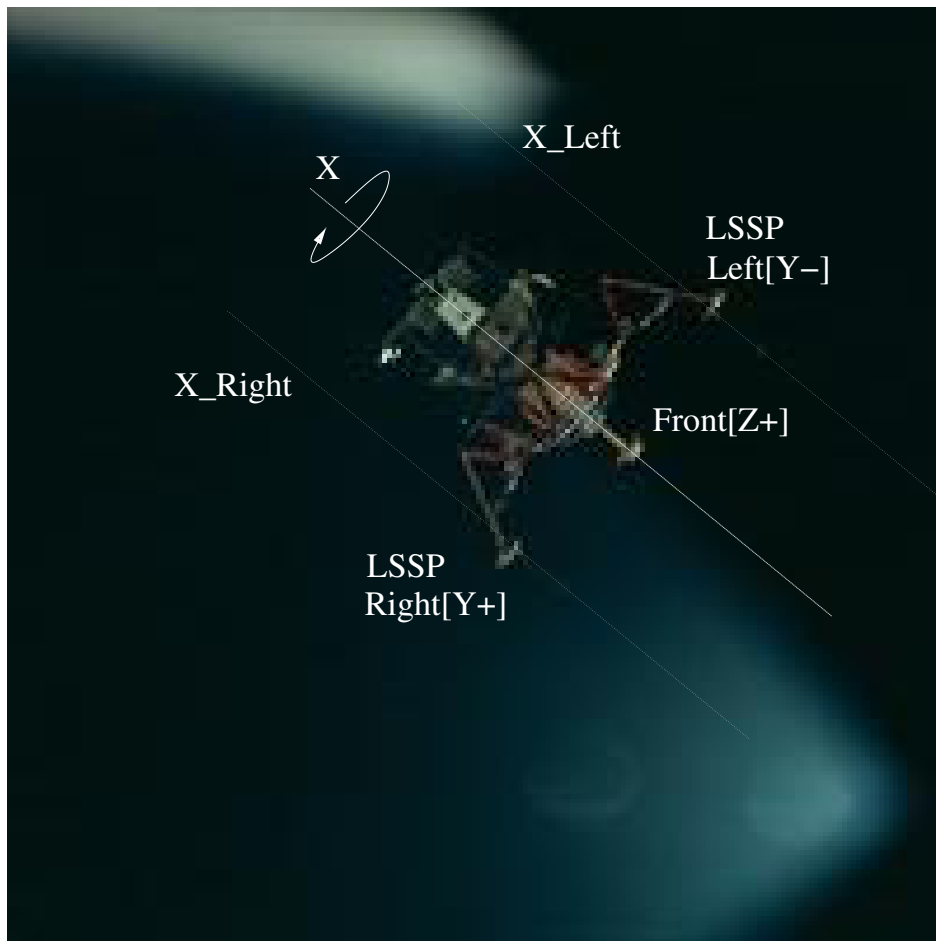


FIG. 17: In the photograph AS11-44-6586, the LM is completing the clockwise 360° yaw. The two landing gears with LSSPs ($Y\pm$) are opposite each other, and flexed inwards rather than being parallel with the LM X-axis.

5. I KNOW YOU CAN'T FAKE IT ANYMORE

We have investigated four scenes from the body of evidence that NASA presented in support of their claim that they flew to the Moon, namely (*i*), the dynamics of Apollo 17 lift-off; (*ii*), the deployment of primary struts during the Moon landing of the Apollo 11 and Apollo 17 missions; (*iii*), the illuminance of the Ascent Stage in the video recording of Apollo 17 of lift-off; and (*iv*), the flexing of the Lunar Surface Sensing Probes during a yaw maneuver in circular Moon orbit prior to descent orbit insertion. We have chosen the scenes based on the physical mechanisms at play were they recorded on the way to the Moon. In all instances we find serious discrepancies between the stresses on the Lunar Module depicted in the scenes and NASA's own performance specifications. In fact, the discrepancies are so great that the findings reported in the previous four sections fully support the alternative explanations of the photographs and of the video recording that emerged in the public in the last two decades, namely, that the pictures of the Apollo 11 Lunar Landing and of the Apollo 17 Lift-off were staged and recorded on Earth.

Acknowledgments

The author acknowledges discussions with anonymous NASA employees to determine when the Lunar Module 360° yaw took place and how much fuel it consumed: In those discussions it was hypothesized that the entries in the Lunar Module Flight Plan for the two yaw burns might have been interchanged by mistake (first of 60°, second of 360°, where the first uses more fuel than the second, see Sec. 4 for full analysis assuming that the log entries are in correct order).

The author acknowledges that the section and subsection titles are titles of or verses from the musical pieces, "Fly Me to the Moon," by Bart Howard (performed by Frank Sinatra), "Let's Twist Again," by Kal Mann and Dave Apell (performed by Chubby Checkers), "Shake a Leg," by AC/DC, "Also Sprach Zarathustra," by Richard Strauss, "Firework," by Katy Perry, "Standing in Motion," by Yanni, and "A New Door," by Lenny Kravitz.

-
- [1] NASA, *Apollo 17 Traverse Planning Data, 3rd Edition*, Fig. 23 on p. 97, [Online; accessed January 18, 2014], URL <https://www.hq.nasa.gov/alsj/a17/A17TraversePlanningData.pdf>.
- [2] NASA, *Apollo 17 Traverse Planning Data, 3rd Edition*, Fig. 7A on p. 15, [Online; accessed January 18, 2014], URL <https://www.hq.nasa.gov/alsj/a17/A17TraversePlanningData.pdf>.
- [3] Smithsonian National Air and Space Museum, *Camera, Television, Lunar Rover, Apollo*, Retrieved May 16, 2014 from http://airandspace.si.edu/collections/artifact.cfm?object=nasm_A19850021000.
- [4] S. T. Thornton and J. B. Marion, *Classical Dynamics of Particles and Systems* (Brooks/Cole, Belmont CA, 2004), chap. 9, 5th ed.
- [5] S. Glasstone, *Sourcebook on the Space Sciences* (D. Van Nostrand Company, Inc., 1965), (Ch. 3).
- [6] J. C. M. IV and J. K. Allred, in *45th AIAA/ASME/ASEE Joint Propulsion Conference and Exhibit* (Denver, Colorado, USA, August 2-5, 2009).
- [7] Apollo News Reference, *Lunar Module Quick Reference Data*, Retrieved June 25, 2015 from https://www.hq.nasa.gov/alsj/LM04_Lunar_Module_ppLV1-17.pdf.
- [8] Wikipedia, *Apollo Lunar Module*, Retrieved April 12, 2015 from https://en.wikipedia.org/wiki/Apollo_Lunar_Module.
- [9] Robert A. Braeunig, *Lunar Module Ascent Simulation* (2009), Retrieved April 11, 2010 from <http://www.braeunig.us/apollo/LM-ascent.htm>, URL <http://www.braeunig.us/apollo/LM-ascent.pdf>.
- [10] Youtube Apollo Houston Channel, *Apollo 17 Lunar Liftoff HD (Inside and Outside view)*, Retrieved June 25, 2015 from <https://www.youtube.com/watch?v=XlGis35Epvs>.
- [11] *Clip Converter - Free Online Media Conversion and Download*, <http://www.clipconverter.cc>.
- [12] The FFmpeg developers, *FFmpeg 2.6.1* (2015), <https://www.ffmpeg.org>.
- [13] Jennifer Levasseur, *Leaving the Moon, Watching at Home* (2011), [Online; accessed January 18, 2014], URL <http://http://blog.nasm.si.edu/history/leaving-the-moon-watching-at-home/>.
- [14] The GIMP Team, *GNU Image Manipulation Program* (2015), <https://www.gimp.org>.
- [15] NASA, *Apollo Operations Handbook - Lunar Module LM 10 and Subsequent - Volume I - Subsystems Data* (1970), [Online; accessed January 18, 2014], URL <https://www.hq.nasa.gov/alsj/alsj-LMdocs.html>.
- [16] ApolloHoax.net, *Topic: Apollo 17 ascent module liftoff* (2014), [Online; accessed January 11, 2015], URL <http://www.apollohoax.net/forum/index.php?topic=655.0>.
- [17] TRW Systems Group, *LMAGS Operating Manual - Flight Program 6* (1969), [Online; accessed January 18, 2014], URL <https://www.hq.nasa.gov/alsj/alsj-LMdocs.html>.
- [18] Ulysse J. Blanchard, *NASA Technical Note D-5029: Full-Scale Dynamic Landing-Impact Investigation of a Prototype Lunar Module Landing Gear* (March 1969), [Online; accessed November 18, 2015], URL

- <http://ntrs.nasa.gov/search.jsp?R=19690011603>.
- [19] William F. Rogers, *NASA Technical Note D-6850: Apollo Experience Report - Lunar Module Landing Gear Subsystem* (June 1972), [Online; accessed November 18, 2015], URL <https://www.hq.nasa.gov/alsj/tnD6850LMLandingGearSubsystem.pdf>.
- [20] Lunar Planetary Institute, *Apollo Image Atlas: 70mm Hasselblad* (1969), [Online; accessed July 13, 2009], URL <http://www.lpi.usra.edu/resources/apollo>.
- [21] Lunar Planetary Institute, *AS11-40-5858* (1969), SHA1SUM: 1515740d4dafb4bde46f00a6b232fe51af573764, URL <http://www.lpi.usra.edu/resources/apollo/images/print/AS11/40/5858.jpg>.
- [22] Lunar Planetary Institute, *AS11-40-5864* (1969), SHA1SUM: f28ca5405b439f543eda84cc64c86992850aeb61, URL <http://www.lpi.usra.edu/resources/apollo/images/print/AS11/40/5864.jpg>.
- [23] Lunar Planetary Institute, *AS11-40-5865* (1969), SHA1SUM: caca091601f6aaace5915d95c8a28768e4d4c7ba5, URL <http://www.lpi.usra.edu/resources/apollo/images/print/AS11/40/5865.jpg>.
- [24] Lunar Planetary Institute, *AS11-40-5921* (1969), SHA1SUM: b899ebaa972c2680ad2e0a6e5fd90e3152ac92bb, URL <http://www.lpi.usra.edu/resources/apollo/images/print/AS11/40/5921.jpg>.
- [25] Lunar Planetary Institute, *AS11-40-5914* (1969), SHA1SUM: 7d1eda076a842c55a240d099373b548b0650cea0, URL <http://www.lpi.usra.edu/resources/apollo/images/print/AS11/40/5914.jpg>.
- [26] Lunar Planetary Institute, *AS11-40-5920* (1969), SHA1SUM: 6e13deef47bddfb9533109af13ff3abcfb400e78, URL <http://www.lpi.usra.edu/resources/apollo/images/print/AS11/40/5920.jpg>.
- [27] NASA, *Apollo 11 Voice Transcripts* (2013), [Online; accessed November 13, 2015], URL <https://www.hq.nasa.gov/alsj/a11/a11.landing.html>.
- [28] Robert F. Stengel, *J. Spacecraft and Rockets* **7**, 941 (1970), Presented as Paper 69-892 at the AIAA Guidance, Control and Flight Mechanics Conference, Princeton, NJ, August 18-20, 1970.
- [29] Lunar Planetary Institute, *AS11-40-5927* (1969), SHA1SUM: 75f51ac6d2fe6f2291f7b72d73a983f7c897d4d5, URL <http://www.lpi.usra.edu/resources/apollo/images/print/AS11/40/5927.jpg>.
- [30] P. T. Metzger, C. D. Immer, C. M. Donahue, B. M. Vu, R. C. Latta, III, and M. Deyo-Svendsen, ArXiv e-prints (2009), Journal reference *J. Aerospace Engineering* Vol. 21, No. 1, January 2009, pp. 24-32, 0906.0196, URL <http://arxiv.org/pdf/0906.0196v1>.
- [31] Lunar Planetary Institute, *AS11-40-5872* (1969), SHA1SUM: 5b7192a7e6b880beddffe8fa5ef9a6a7e97ace0b, URL <http://www.lpi.usra.edu/resources/apollo/images/print/AS11/40/5872.jpg>.
- [32] F. Pitié, Master's thesis, Trinity College, Dublin, Ireland (2002), [Online; accessed January 11, 2015], URL <http://citeseerx.ist.psu.edu/viewdoc/download?doi=10.1.1.1.1574.pdf>.
- [33] NASA, *Apollo Flight Journal: Day 5, part 2: Undocking and the Descent Orbit* (Last updated 2013-08-11), [Online; accessed January 18, 2014], URL <http://http://history.nasa.gov/ap11fj/15day5-undock-doi.htm>.
- [34] Lunar Planetary Institute, *AS11-44-6586* (1969), SHA1SUM: 51e276ad58b1ad1c738f0d89eae690ca9e0ec713, URL <http://www.lpi.usra.edu/resources/apollo/images/print/AS11/44/6586.jpg>.
- [35] Lunar Planetary Institute, *AS11-44-6575* (1969), SHA1SUM: 7698cc-

- fab214c3aca045ae1d8ce40ef7be8bb9bf, URL <http://www.lpi.usra.edu/resources/apollo/images/print/AS11/44/6575.jpg>.
- [36] Lunar Planetary Institute, *AS11-44-6576* (1969), SHA1SUM: 776f462ac9f082d71a98d5ed5570c4184fcedbe3, URL <http://www.lpi.usra.edu/resources/apollo/images/print/AS11/44/6576.jpg>.
- [37] Lunar Planetary Institute, *AS11-44-6577* (1969), SHA1SUM: 79e913ca016c445b673d0d7df7dcd595e5e45f5b, URL <http://www.lpi.usra.edu/resources/apollo/images/print/AS11/44/6577.jpg>.
- [38] Lunar Planetary Institute, *AS11-44-6578* (1969), SHA1SUM: 14a2d98a627cd6e6bf07a25a5d6700509c948dc6, URL <http://www.lpi.usra.edu/resources/apollo/images/print/AS11/44/6578.jpg>.
- [39] Lunar Planetary Institute, *AS11-44-6579* (1969), SHA1SUM: 183798d022bf1349ff58822c562dd3bb9e9b1dc6, URL <http://www.lpi.usra.edu/resources/apollo/images/print/AS11/44/6579.jpg>.
- [40] Lunar Planetary Institute, *AS11-44-6580* (1969), SHA1SUM: ba78d904864570e10d0534b5ecdc043cd0868ce4, URL <http://www.lpi.usra.edu/resources/apollo/images/print/AS11/44/6580.jpg>.
- [41] Lunar Planetary Institute, *AS11-44-6581* (1969), SHA1SUM: 7519de3468bf605b6ba8487e8ce5bd199ae81196, URL <http://www.lpi.usra.edu/resources/apollo/images/print/AS11/44/6581.jpg>.
- [42] Lunar Planetary Institute, *AS11-44-6582* (1969), SHA1SUM: 95a988a07b8997570eedd8a2ed366b16d39a3636, URL <http://www.lpi.usra.edu/resources/apollo/images/print/AS11/44/6582.jpg>.
- [43] Lunar Planetary Institute, *AS11-44-6583* (1969), SHA1SUM: bc34471a18838d4a7ef3274e3172bf802429ca70, URL <http://www.lpi.usra.edu/resources/apollo/images/print/AS11/44/6583.jpg>.
- [44] Lunar Planetary Institute, *AS11-44-6584* (1969), SHA1SUM: 0c4c7fb13a80a7606f7c9faed26ffada32cbb8d6, URL <http://www.lpi.usra.edu/resources/apollo/images/print/AS11/44/6584.jpg>.
- [45] Lunar Planetary Institute, *AS11-44-6585* (1969), SHA1SUM: 26f4c032d391bc692e8499e114293039ac13be83, URL <http://www.lpi.usra.edu/resources/apollo/images/print/AS11/44/6585.jpg>.
- [46] Created using command line interface as follows,

```
ffmpeg -i Apollo_17_Lunar_Liftoff_high.avi -q:v 1 -r 10 image-%05d.jpg
```
- [47] We use `matlab` notation throughout the report where “:” is used to designate integer range first number to second number, inclusive of the boundaries. E.g., in that notation `[100 : 102]` represents an array `[100, 101, 102]`.
- [48] Created using command line interface as follows,

```
ffmpeg -i Apollo_17_Lunar_Liftoff_high.avi -q:v 1 -r 25 image-%05d.jpg
```